

Phase Equilibration and Magnetic Field Generation in U(1) Bubble Collisions

E. J. Copeland^a, P. M. Saffin^b and O. Törnkvist^c

^a*Centre for Theoretical Physics, University of Sussex,
Brighton BN1 9QH, United Kingdom*

^{b,c}*Department of Applied Mathematics and Theoretical Physics,
University of Cambridge,
Cambridge CB3 9EW, United Kingdom*

July 17, 1999

Abstract

We present the results of lattice computations of collisions of two expanding bubbles of true vacuum in the Abelian Higgs model with a first-order phase transition. New time-dependent analytical solutions for the Abelian field strength and the phase of the complex field are derived from initial conditions inferred from linear superposition and are shown to be in excellent agreement with the numerical solutions especially for the case where the initial phase difference between the bubbles is small. With a step-function approximation for the initial phase of the complex field, solutions for the Abelian field strength and other gauge-invariant quantities are obtained in closed form. Possible extensions of the solution to the case of the electroweak phase transition and the generation of primordial magnetic fields are briefly discussed.

^aElectronic address: e.j.copeland@sussex.ac.uk

^b Electronic address: p.m.saffin@damtp.cam.ac.uk

^c Electronic address: o.tornkvist@damtp.cam.ac.uk

1 Introduction

Phase transitions are a universal feature in field theories. For example, they may explain how quark confinement has emerged and possibly how the electroweak symmetry was broken. It is also through such transitions that topological defects form in condensed-matter systems in the laboratory and, we believe, could have formed in the early universe (see [1] and [2] for reviews). Phase transitions of the first order play a particularly significant role in particle cosmology, either as a progenitor of inflation [3, 4, 5] or as a source of the baryon asymmetry associated with the electroweak transition [6]. Popular models of electroweak physics such as the Minimal Supersymmetric Standard Model exhibit a first-order transition for a range of experimentally allowed parameters [7]. First-order phase transitions are driven by the nucleation of bubbles of true vacuum within a sea of false vacuum. The bubbles, responding to the pressure caused by the energy difference of the two vacua, expand and subsequently collide. Over the years, a number of authors have turned their attention to the dynamics of such bubble collisions in gauge theories [8, 9, 10, 11, 12, 13]. In spite of this effort, it is fair to say that much remains unclear about the role the various fields play in the collision process. This should not be surprising, as we are here dealing with a non-linear system which is difficult to treat analytically.

Much of the interest in bubble collisions derives from the pioneering work of Kibble [14], who demonstrated the possible formation of topological defects in a cosmological phase transition for cases where the vacuum manifold of the Higgs potential is non-trivial. In particular, defects such as strings (or monopoles) may be produced in the collision of three (four) bubbles, provided that inside each bubble the scalar Higgs field takes a different random value on the vacuum manifold. In Ref. [14] the mechanism for defect formation was formulated in terms of a geodesic rule, according to which the phase (or, more generally, the isospace orientation) of the scalar field between two colliding bubbles takes values along the shortest path on the vacuum manifold that connects the values in each bubble. The geodesic rule has since been verified for defect formation in various models with broken global symmetry [15, 16]. In gauge theories, however, Rudaz and Srivastava [9] have argued that the geodesic rule does not apply, since the phase of the scalar field has no gauge-invariant meaning. Instead, they suggested that the dynamics of the fields would play an important role in the production of gauge defects in a first-order phase transition and could possibly lead to a suppression in the rate of defect formation.

This claim was subsequently investigated by Hindmarsh, Davis, and Brandenberger [10]. Assuming the gauge fields to be negligible at the moment of collision, they obtained solutions which appeared to adhere to the prescription of the (naive) geodesic rule and found no suppression in the probability of defect formation. Later, however, Copeland

and Saffin [12] demonstrated unequivocally that the geodesic rule can be violated in a $U(1)$ gauge theory as a consequence of the detailed energetics in bubble collisions. The reason is that violent fluctuations in the modulus of the scalar field cause symmetries to be restored locally, allowing the phase to “slip” by an integer multiple of 2π and thus change the number of string defects. In fact, when the initial phase difference of the bubbles and their initial separation are sufficiently large, string defects can arise when only two bubbles collide, unlike the usual picture of string formation obeying the geodesic rule, which would require at least three bubbles. In this article, however, we will be dealing with phase differences and bubble separations which are too small to cause defects to form through violation of the geodesic rule.

An appealing aspect of first-order transitions involving gauge fields is that the bubble collisions give rise to magnetic fields. These are produced by a gauge-invariant current which develops across the surface of intersection of the two bubbles due to the gradient of the phase of the scalar field [11]. Because bubble collisions occur out of thermal equilibrium and the bubble walls possess large kinetic energy, the magnetic fields thus created can be considerably larger than the thermal background of magnetic-field fluctuations. If the energetics permits the geodesic rule to be violated, these magnetic fields become associated with the formation of local (gauged) defects.

Magnetic fields could also be generated in extensions of the $SU(2)\times U(1)$ Standard Model with a first-order phase transition and have been studied by a number of authors [17, 18, 19]. Such fields, created in the early universe, could evolve into seed fields for a galactic dynamo mechanism that would in turn amplify them to the strength observed in galaxies today. The common view has been that it is generally too difficult to produce large enough fields at the electroweak phase transition on sufficiently large length scales, but recently Davis, Lilley and Törnkvist [20] have argued that in the context of a universe with less matter than the critical density (and particularly with a positive cosmological constant) a much smaller primordial field would be sufficient for explaining the present galactic fields. The reason is simple: The increased age of galaxies in such a universe gives the primordial seed field more time to grow in strength.

In this article we shall concentrate on the case of the $U(1)$ Higgs model, partly to simplify the analysis but also to compare our results with those of Kibble and Vilenkin [11], who developed a formalism for calculating the magnetic fields generated in bubble collisions. Of course, one should not really call it a magnetic field in the case of an Abelian gauge theory, owing to the lack of a massless photon in the broken-symmetry phase. Instead we will generally refer to it as a “field strength”. The authors of Ref. [11] made some potentially severe approximations in order to solve the field equations: The modulus of the complex Higgs field was kept fixed in the true vacuum, and the initial phase of the Higgs field at the moment of collision was approximated by a step function.

With these basic assumptions, they were able to derive some fascinating analytical results concerning the generation of the field strength in the collision region. They demonstrated how the gauge-invariant current across the interface of the two colliding bubbles produces a ring of flux of the Abelian field strength which encircles the bubble intersection region. On top of this they defined a gauge-invariant phase difference between the two bubbles and solved for its future evolution to show that it oscillates and eventually relaxes to zero as the bubbles merge. This example of phase equilibration between two colliding bubbles is in fact a generic feature of models with either local or global symmetry [11, 21].

Here we go beyond the approximations introduced in Ref. [11] and, by doing so, test their regime of validity. In particular, we allow for a smoother interpolation of the phase between the two bubbles, using an approximation to the bounce solution for a single bubble, and the fact that we can represent the scalar field of two well separated bubbles as a linear superposition of the scalar fields for each bubble [10, 13]. Remarkably, we can obtain explicit time-dependent expressions for both the gauge-invariant phase and the Abelian field strength. We compare these expressions to those in Ref. [11] as well as to the numerical solution of the field equations. The results are very encouraging; we find incredible agreement between our analytical solutions and the numerical solutions. We also demonstrate to what extent fields in the collision region are well approximated by the step-function ansatz adopted in Ref. [11].

Real phase transitions naturally possess lots of complicating factors which we do not take into account here, such as frictional damping of the bubble-wall velocity. Particles that acquire a mass due to couplings to the Higgs field are massless outside the bubble and massive inside. Not all the particles external to the bubble have enough energy to become massive and must reflect off the bubble wall, slowing it down [21, 22, 23].

Another complication is the conductivity associated with the plasma surrounding the expanding bubble wall. Charged particles in the plasma couple to the gauge fields and cause them to lose their energy to the thermal bath. This has the effect of reducing the likelihood of forming loops of flux during the bubble collision as pointed out in [10, 11] and confirmed in [12]. Furthermore, the existence of a highly conductive plasma has the effect of conserving magnetic flux by virtue of Faraday's and Ohm's laws.

In spite of these potential problems, we believe that the simple system of colliding bubbles is well worth investigating, not least because the field theory is highly non-linear and yet we are able to find extremely accurate analytical solutions. Moreover, as we shall discuss in the conclusions, the method and results can be generalised and applied to different areas, such as the Standard Model and its extensions.

The paper is organised as follows. In Sec. 2 we review the standard results due to Coleman [24] on bounce solutions and bubble nucleation in first-order phase transitions. Following Ref. [25], we also investigate the evolution of bubbles of arbitrary nucleation

radius and find that all expanding bubbles are well approximated by the bounce solution after the bubble size has increased only by a small amount. In Sec. 3 we review the key approximations and results obtained in Ref. [11], in particular the solutions for the gauge-invariant phase and the field strength arising from the step-function approximation. We rewrite these solutions, and solutions for other gauge-invariant quantities, as closed-form expressions in terms of Bessel functions. In Sec. 4 we obtain improved solutions by using the smooth bounce solution for the scalar field of each individual bubble and the linear superposition ansatz for the combined scalar field. We derive explicit time-dependent solutions for the gauge-invariant phase and the Abelian field strength. The numerical lattice computation is described in Sec. 5. In Sec. 6 we compare the numerical field evolution to our new smooth solution and to the results obtained in Ref. [11]. Of particular note is that the step-function approximation leads to discontinuities in the field strength and in the phase that are not there in the smooth approximation. Moreover, the energy density associated with the gauge field arising from the step-function approach is about sixteen times larger than the true solution found both numerically and in the smooth approximation. We conclude in Sec. 7.

2 Kinematics of Expanding Spherical Bubbles

In a pioneering paper Coleman [24] investigated the physics of bubble nucleation in the decay of the metastable vacuum. He obtained the so-called bounce solution for the modulus of the scalar field corresponding to a single nucleated bubble. If the bubble radius is large compared to the wall thickness, the bubble wall can equivalently be described as a relativistic membrane. The motion of such a membrane subjected to the outward pressure caused by the energy difference of the two vacua can be derived and was investigated in the spherical case by Garriga [25]. Below we will reproduce a number of key results in Refs. [24, 25], extracting details of the bubble-wall dynamics that we shall require later. Of particular use will be an analytic approximation, Eq. (6), to the actual bounce solution, Eq. (5), as well as the most probable size of the nucleated bubble, Eq. (10), and the associated wall thickness, Eq. (11).

We shall see below that bubbles created via an instanton description of tunnelling have $O(1,3)$ symmetry. When there are two bubbles present the spatial rotation symmetry is reduced to $O(2)$, so in fact the two-bubble collision has an $O(1,2)$ symmetry [8]. When we have two bubbles there is the chance that they may nucleate at different times and so have different sizes when they collide. We may however always boost to a frame where they nucleate simultaneously; this is the frame in which we shall work.

2.1 Bubble Nucleation

For simplicity we choose a Higgs potential¹ that is cubic in $\phi^*\phi$ [8]:

$$V(|\phi|) = \lambda(|\phi|^2 - \eta^2)^2 \left(\frac{|\phi|^2}{\eta^2} + \epsilon \right) - \epsilon\lambda\eta^4, \quad (1)$$

where ϕ is the scalar Higgs field and $0 < \epsilon < \frac{1}{2}$. It has a metastable minimum at $\phi = 0$ and a degenerate global minimum at $\phi = \eta e^{i\theta}$, $\theta \in [0, 2\pi)$, separated by a barrier of height $[4(1 + \epsilon)^3/27 - \epsilon]\lambda\eta^4$. The difference in energy density between the two minima is $p = \epsilon\lambda\eta^4$, and this constant has been subtracted in Eq. (1) in order to obtain zero energy density in the metastable minimum. The Higgs-boson mass M_H in this model is given by $M_H^2 = 4(1 + \epsilon)\lambda\eta^2$.

The nucleation of a bubble of true Higgs vacuum $|\phi| = \eta$ occurs by means of tunnelling from $\phi = 0$ through the barrier [24]. The tunnelling is expected to be dominated by solutions to the Euclidean equations of motion, with a nucleation probability $\propto \exp(-S_E)$, where S_E is the Euclidean action. S_E is given by

$$S_E[\phi, A_\mu] = \int d^4\bar{x} \left[|D_\mu\phi|^2 + V(|\phi|) + \frac{1}{4}F_{\mu\nu}F^{\mu\nu} \right], \quad (2)$$

where a positive definite metric is used. The covariant derivative is $D_\mu = \partial_\mu + ieA_\mu$ with $F_{\mu\nu} = \partial_\mu A_\nu - \partial_\nu A_\mu$, and A_μ is the associated U(1) vector potential. Tunnelling is therefore dominated by those instantons with lowest Euclidean action, something which is achieved by having vanishing vector potential and a constant phase for the scalar field ϕ .

In the absence of gauge fields the instantons which have lowest action (2) are those with O(4) symmetry, i.e. $\phi = \phi(s)$, where $s = \sqrt{t_E^2 + \mathbf{x}^2}$ and $t_E = it$ is the Euclidean time coordinate. In fact, all other solutions to the Euclidean equations are divergent [26]. In considering the nucleation of one isolated bubble we may, without loss of generality, choose ϕ to be real and non-negative. For such configurations the ϕ equation of motion is

$$\frac{1}{s^3} \frac{d}{ds} \left(s^3 \frac{d\phi}{ds} \right) = \frac{1}{2} \frac{dV}{d\phi}. \quad (3)$$

The “bounce” solution [24] to this equation satisfies the boundary conditions $\phi'(0) = 0$, $\phi(\infty) = 0$ and is characterised by a kink, the bubble wall, localised near $s = R_0$, where R_0 is to be determined. For $\epsilon \ll 1$, R_0 turns out to be large compared to the width

¹We remark that the choice of potential is not important, and that the phenomena discussed in this article are qualitatively similar for any effective potential exhibiting a first-order phase transition. The quantitative results will be seen to depend on generic features of the potential, such as barrier height, the location of the two minima, and their difference in energy density.

of the kink, so one can set $s \approx R_0$ in the region where $d\phi/ds$ differs significantly from zero. Moreover, for small ϵ we have $V(\phi) \approx V_0(\phi)$, where $V_0(\phi)$ is obtained from $V(\phi)$ by setting $\epsilon = 0$, and $\phi(0) \approx \eta$. With these approximations, collectively known as the “thin-wall” approximation, Eq. (3) is easily integrated to yield

$$\frac{d\phi}{ds} = -\sqrt{V_0(\phi)} . \quad (4)$$

After one further integration one obtains the bounce solution particular to our potential,

$$\phi_b(s) = \frac{\eta}{\sqrt{2}} \left[1 - \tanh \left(\eta \sqrt{\lambda} (s - s_0) \right) \right]^{\frac{1}{2}} , \quad (5)$$

where a constant of integration s_0 appears because the boundary condition $\phi'(0) = 0$ is not exactly satisfied in the thin-wall approximation. The bounce profile is centred at the value of s for which $\phi_b = \eta/2$, i.e. $s = R_0 \equiv s_0 + \operatorname{arccoth}(2)/(\eta\sqrt{\lambda})$. Near $s = R_0$ the bounce solution is well approximated by

$$\phi_b(s) \simeq \frac{\eta}{2} [1 - \tanh 2\mu_0(s - R_0)] , \quad (6)$$

where

$$\mu_0 \equiv -\frac{1}{\eta} \phi_b'(R_0) = \frac{1}{\eta} \sqrt{V_0(\eta/2)} = \frac{3\eta\sqrt{\lambda}}{8} \approx \frac{3M_H}{16} \quad (7)$$

by virtue of Eq. (4). Asymptotically, however, the approximation (6) differs from the solution (5). Whereas the latter tends to zero as $\phi_b \sim \exp(-\eta\sqrt{\lambda}s)$ for $s \rightarrow +\infty$ and tends to η as $(\eta - \phi_b) \sim \exp(2\eta\sqrt{\lambda}s)$ for $s \rightarrow -\infty$, the approximation (6) instead approaches both these asymptotic values as $\sim \exp(-3\eta\sqrt{\lambda}|s|/2)$. Fig. 1 shows a comparison of the analytical approximations of the bounce profile given in Eqs. (5) and (6) with the numerical solution of Eq. (3).

The nucleation radius R_0 is as yet undetermined, but can be calculated by extremising the Euclidean action. For the bounce solution in the absence of gauge fields this action can be calculated using the thin-wall approximation and Eq. (4) without reference to the solution itself. One obtains

$$S_E \simeq 2\pi^2 \left(\sigma R_0^3 - \frac{1}{4} p R_0^4 \right) , \quad (8)$$

where

$$\sigma = \int_0^\infty ds \left[\left(\frac{d\phi}{ds} \right)^2 + V(\phi) \right] \simeq 2 \int_0^\eta d\phi \sqrt{V_0(\phi)} = \eta^3 \sqrt{\lambda}/2 , \quad p = \lambda \epsilon \eta^4 . \quad (9)$$

Here σ is the surface tension, or mass per unit area, of the bubble wall, whereas the outward pressure p is equal to the difference in energy density between the metastable

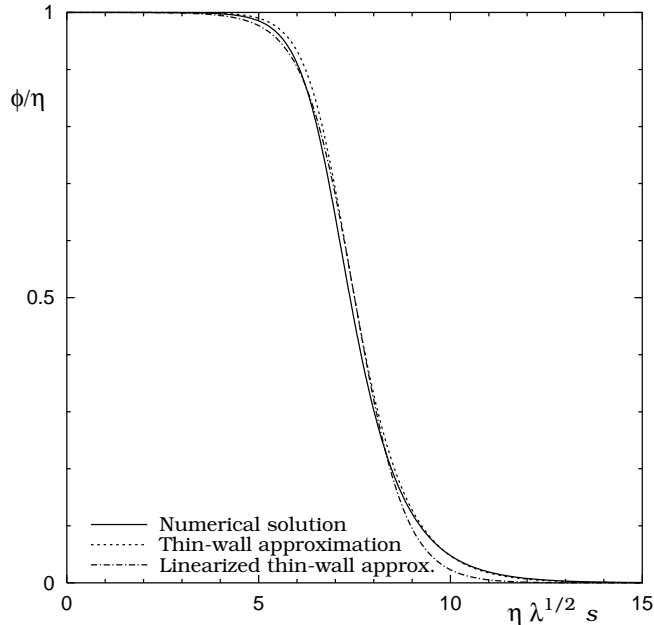


Figure 1: Bounce profiles for $\epsilon = 0.2$. Here are shown the exact solution of Eq. (3) (solid), the thin-wall approximation given by Eq. (5) (dotted), and the “linearized” thin-wall approximation given by Eq. (6) (dot-dashed).

and global minima. The factor $2\pi^2 R_0^3$ in Eq. (8) is the area of the three-sphere, whilst $2\pi^2 R_0^4/4$ is the four-volume of the instanton. The action S_E is extremised by the value,

$$R_0 = \frac{3\sigma}{p} = \frac{3}{2\epsilon\eta\sqrt{\lambda}}. \quad (10)$$

The initial conditions for the evolution of a bubble is given by the $t_E = 0$ slice of the instanton, along which $\partial\phi_b/\partial t_E = 0$, such that the bubble is initially stationary. The future evolution is found by analytically continuing the bounce solution to Minkowski space; details may be found in Ref. [24].

The thin-wall limit allows us to make statements about the evolution as well as the nucleation of bubbles. A measure of the bubble-wall thickness is provided by μ^{-1} , where

$$\mu \equiv -\frac{1}{\eta} \frac{d\phi_b}{dr} \Big|_{s=R_0} = \mu_0 \frac{r(t)}{R_0} = \frac{\mu_0}{\sqrt{1-\dot{r}^2}}, \quad \dot{r} \equiv \frac{dr(t)}{dt} \quad (11)$$

showing that the thickness of the bubble wall is subject to the expected Lorentz contraction. The thickness μ_0^{-1} at $t = 0$ is given in the thin-wall approximation by Eq. (7). By

means of Eqs. (7) and (10) the condition for the thin-wall approximation to be valid can be stated

$$\mu_0 R_0 = \frac{9}{16\epsilon} \gg 1 . \quad (12)$$

2.2 Spherical Membrane Dynamics

Bubbles whose time evolution is not O(1,3) symmetric are nucleated, but with lower probability, as the result of tunnelling via instantons that do not extremise the Euclidean action. In particular, such bubbles may deviate from spatial spherical symmetry, or they may be spherically symmetric but not invariant under boosts. We shall here consider the latter possibility.

When the bubble wall is thin compared to the radius of the bubble, it can be approximated by an infinitely thin membrane. The equation for the radius $r(t)$ of a spherical membrane subject to an outward pressure can be written [25]

$$\frac{dE}{dt} = 0 , \quad E \equiv \frac{\sigma}{\sqrt{1 - \dot{r}^2}} r^2 - \frac{1}{3} p r^3 , \quad (13)$$

where $\dot{r} = dr/dt$, σ is the surface tension, or mass per unit area, of the membrane and p is the difference in energy density between the false vacuum exterior to the bubble and the true vacuum inside. Equation (13) simply expresses the conservation of energy, but can also be obtained as a special case of the motion of a relativistic membrane in an external force field. Because of the relativistic factor $(1 - \dot{r}^2)^{-1/2}$ the first term of E comprises the total energy of the bubble wall, mass as well as kinetic energy, while the second term is the total energy of the true vacuum inside the bubble. The general solution $r(t)$ is given implicitly as

$$\int_{r(0)}^{r(t)} dr \frac{3E + p r^3}{\sqrt{(3E + p r^3)^2 - 9\sigma^2 r^4}} = \pm t . \quad (14)$$

In the special case $E = 0$, one obtains an explicit solution with O(1,3) symmetry,

$$r^2 - t^2 = R_i^2 , \quad R_i = r(0) . \quad (15)$$

If the bubble is nucleated at rest at $t = 0$, we have from Eq. (13) that its initial radius is $R_i = R_0 \equiv 3\sigma/p$. Equation (15) then coincides with the equation of motion for the centre of the bubble wall in the O(1,3) Wick-rotated bounce solution considered above.

A set of bubble-wall trajectories for different values of E are depicted in Fig. 2. The bubbles are all chosen to start from rest at $t = 0$. If the initial radius R_i is smaller than the critical radius $R_{\text{crit}} = 2\sigma/p = (2/3)R_0$, the bubble recollapses, whereas if $R_i > R_{\text{crit}}$, it expands. Only the trajectory with $R_i = R_0$ is a hyperbola, corresponding to the O(1,3) symmetry. It should be noted that, although the initial expansion for $R_i > R_{\text{crit}}$

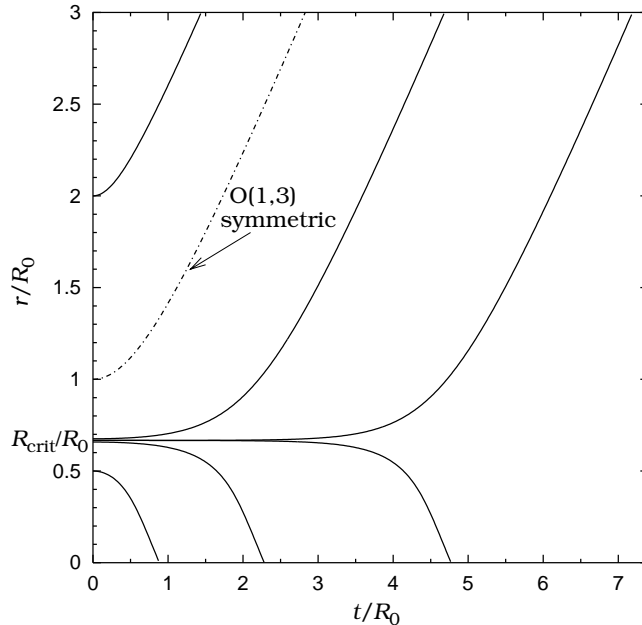


Figure 2: Evolution of the radius of spherical bubbles nucleated at rest in a first-order phase transition. $R_0 = 3\sigma/p$.

takes place on different timescales, once the bubble radii have increased by about $R_0/2$ the remaining evolution is quite well approximated by a time-translated $O(1,3)$ solution. Therefore, if the average distance between nucleation sites is larger than about $3R_0$, the $O(1,3)$ -symmetric solution will generally provide a good description of expanding bubbles at the time of their collision.

3 Bubble Collisions and the Kibble-Vilenkin Approximation

We now proceed to study collisions of two expanding bubbles of true vacuum. As was argued in Sec. 2.1, for typical bubbles the phase of the complex field inside each bubble is (covariantly) constant, and we may initially choose a gauge in which the gauge vector potential vanishes everywhere. Then there will in general be a random initial phase difference $\Delta\theta_0$ between the two bubbles.

It was shown by Kibble and Vilenkin [11] that, because of the phase difference, a gauge-invariant current $j_k = ie[\phi^* D_k \phi - (D_k \phi)^* \phi]$ develops across the surface of inter-

section of the two bubbles as they collide. The current gives rise to a ring-like flux of the Abelian field strength F_{ij} which takes the shape of a girdle encircling the bubble intersection region. Moreover, these authors showed that, under the assumptions that the radial mode of the scalar field is strongly damped and a step function can be used to approximate the initial phase of the complex field at the moment of collision, the phase oscillates and equilibrates to a uniform value as the bubbles merge.

We shall here review briefly the approach of Ref. [11], as it forms a common basis for the analytical methods discussed and developed in this article. We will analyse the results arising from their approximation and derive closed-form expressions for gauge-invariant quantities such as the Abelian field strength. Crude estimates are extracted for the peak value of the field strength and the scale of spatial variation of the field. These quantities are relevant for determining the strength and correlation length of magnetic fields that may be created through bubble collisions in the early universe in more realistic models.

Let us consider two non-overlapping bubbles, each locally $O(1,3)$ symmetric with respect to a frame with origin at its centre. The separation of their nucleation events is then necessarily spacelike, and one may pick a reference frame and coordinate origin such that they are nucleated simultaneously with centres at $(t, x, y, z) = (0, 0, 0, \pm R_c)$. In this frame, the bubbles have equal initial radius $R_i = R_0$. Their first collision occurs at $(t_c, 0, 0, 0)$ when their radii are R_c and $t_c = \sqrt{R_c^2 - R_0^2}$ by virtue of Eq. (15).² The system of two bubbles has the invariance $O(1,2)$ reducing the problem to a $1 + 1$ dimensional one that can be expressed in terms of the coordinates z and τ , where

$$\tau^2 = t^2 - x^2 - y^2 . \quad (16)$$

In these coordinates the point of first contact $z = 0, \tau = t_c$ (denoted by C in Fig. 3b) represents the worldsheet of the circle of most recent intersection of the bubble walls in $3+1$ dimensional spacetime. This circle recedes superluminarily from the z axis according to the equation $x^2 + y^2 = \rho_c^2 \equiv t^2 - t_c^2, t \geq t_c$. Its position at a particular time t is indicated by the label C_t in Fig. 3a.

Let us write the scalar Higgs field in polar form $\phi = X e^{i\theta}$. In the axial gauge $A_z = 0$ its modulus, phase, and the vector potential take the form

$$X = X(\tau, z), \quad \theta(x) = \theta_a(\tau, z), \quad A^\alpha(x) = x^\alpha a(\tau, z) , \quad (17)$$

where $\alpha \in \{0, 1, 2\}$. The condition $\theta_a(\tau, 0) = 0$ fixes the gauge completely.

Following Ref. [11] the modulus X of the scalar field inside the bubbles and in their overlap region is approximated by the constant true-vacuum value η . The equations for

²Unlike Ref. [11] we do not assume that $t_c/R_c = 1$, which would be approximately true only if $R_c \gg R_0$.

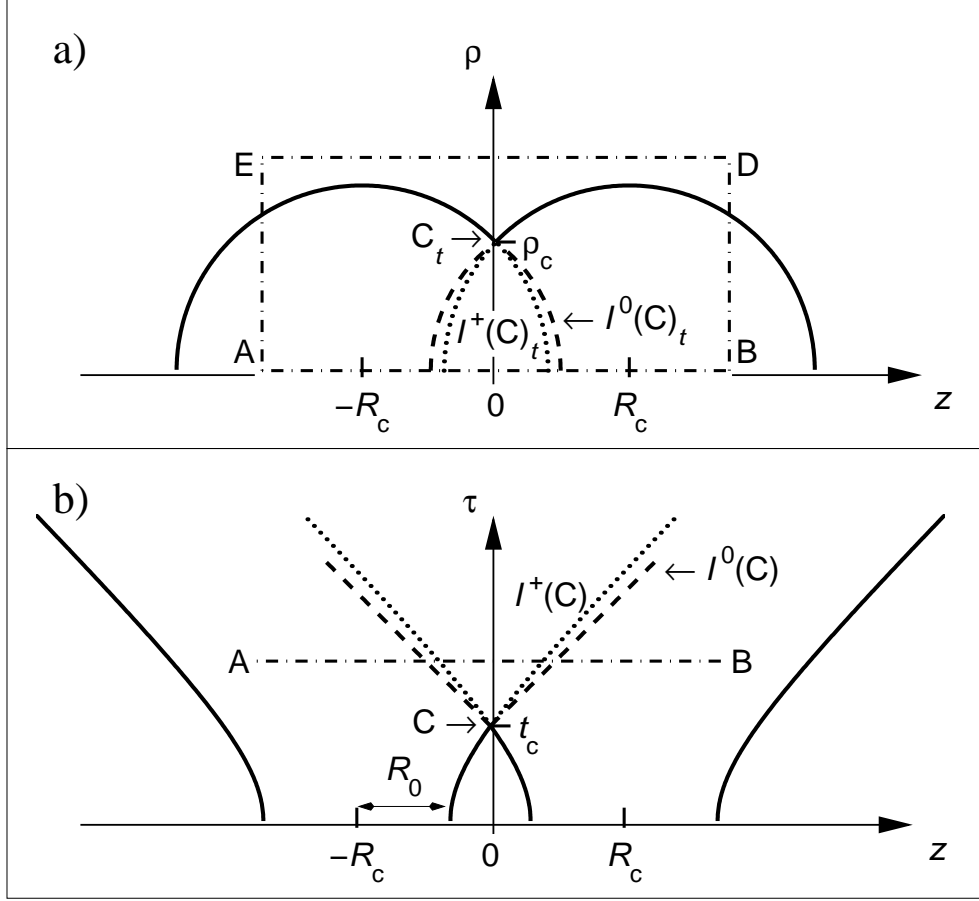


Figure 3: Bubble collision in two different coordinate systems. Dotted curves indicate the extrapolated position of each bubble wall in the absence of a collision. The union of causal futures of bubble-wall intersections, $I^+(C)$, extends out to the causal horizon $I^0(C)$ drawn as a dashed curve, and is the only region where physical fields that result from bubble collision events can exist. Further notation is explained in the text. (a) Slice of bubble collision for constant time t and constant azimuthal variable φ . Here C_t denotes the instantaneous position of the circle of most recent intersection, whose radius is ρ_c . The contour $ABDEA$ is used for evaluating the Abelian flux. (b) Reduced spacetime diagram of entire bubble collision. The point C represents all intersections of the two bubble walls.

$\theta_a(\tau, z)$ and $a(\tau, z)$ then reduce to the linear equations

$$\partial_\tau^2 \theta_a + \frac{2}{\tau} \partial_\tau \theta_a - \partial_z^2 \theta_a + m^2 \theta_a = 0 , \quad (18)$$

$$\partial_\tau^2 a + \frac{4}{\tau} \partial_\tau a - \partial_z^2 a + m^2 a = 0 , \quad (19)$$

together with

$$3a + \tau \partial_\tau a = \frac{m^2}{e} \theta_a , \quad (20)$$

where m is the vector-boson mass, $m^2 = 2e^2 \eta^2$. The constant-modulus approximation is not quite consistent, as nontrivial solutions of Eqs. (18) and (19) do not satisfy the remaining equation

$$\square X - (D_\mu \theta D^\mu \theta) X + \frac{1}{2} \frac{dV}{dX} = 0 \quad (21)$$

for constant $X \equiv \eta$. On the contrary, non-trivial gauge-invariant phase gradients $D_\mu \theta \equiv \partial_\mu \theta + e A_\mu$ appear inside the causal future of bubble-wall intersections $I^+(\text{C}) = \{(z, \tau) | \tau - t_c > |z|\}$ (see Fig. 3b) and serve as sources for fluctuations in the Higgs-field modulus. Fortunately, for a small initial phase difference $\Delta\theta_0$ the fluctuations in X are also small, so that Eqs. (18), (19) and (20) remain a good approximation for the phase and the vector potential.

In this article we shall be interested mainly in two quantities, the Abelian field strength $F^{\alpha z} = x^\alpha \partial_z a(\tau, z)$ and the phase θ of the complex field. The field strength is gauge invariant, but the phase is not. Because the analytical treatment simplifies in the axial gauge, while the lattice computations of Sec. 5 are conveniently performed in the temporal gauge, it is useful to construct a gauge-invariant generalisation of the phase θ which can be calculated in either gauge, so that the independent results may be compared. Such a gauge-invariant phase can be defined [11] at any point P by means of the line integral of the gauge-invariant phase gradient $D_\mu \theta \equiv \partial_\mu \theta + e A_\mu$ from the origin to P. Unfortunately, this line integral is path dependent. In this work we shall fix the definition of the gauge-invariant phase $\tilde{\theta}$ by specifying a path from the origin as follows:

$$\tilde{\theta}(\tau, z) \equiv \int_{(0,0,0,0)}^{(t,x,y,0)} dx^\alpha D_\alpha \theta + \int_{(t,x,y,0)}^{(t,x,y,z)} dz D_z \theta , \quad (22)$$

where $\alpha = 0, 1, 2$ is summed over. By choosing initial conditions for Eqs. (18) and (19) (or the full, nonlinear equations) that adhere to the symmetry of the problem, one can arrange for the solution to be such at all times that $\partial_\alpha \theta$ and A_α are both odd functions of the variable z . Then the first term of Eq. (22) does not contribute, and we have

$$\tilde{\theta}(\tau, z) \equiv \int_{(\tau,0)}^{(\tau,z)} dz D_z \theta(\tau, z) . \quad (23)$$

The expression simplifies further in the axial gauge $A_z = 0$, where one finds $\tilde{\theta}(\tau, z) \equiv \theta_a(\tau, z)$. Note that, while $D_\mu \theta$ is defined locally, the phase $\tilde{\theta}$ is a non-local quantity by construction. Therefore, it is not a physical variable, and the evolution of $\tilde{\theta}$ exhibits non-causal correlations. Nevertheless, $\tilde{\theta}$ provides a useful, gauge-invariant characterisation of the field configuration.

3.1 Step-Function Approximation

In the approach by Kibble and Vilenkin [11], a sign function is used³ to approximate the initial phase difference between the two bubbles at the instant when they collide, $\tau = t_c$. This would correspond to bubbles with infinitely thin walls. The initial conditions on the phase and its derivative are taken to be $\theta_a(t_c, z) = \theta_0 \text{sgn}(z)$, corresponding to a phase difference of $\Delta\theta_0 = 2\theta_0$, and $\partial_\tau \theta_a(t_c, z) = 0$. The vanishing of the derivative can be understood from Fig. 3b, since at $\tau = t_c$ points with $|z| > 0$ are in the interior of bubbles with constant phase $\pm\theta_0$, and $\theta_a(\tau, 0) = 0$ from the gauge condition. In this ansatz, the bubbles are treated as though they extend to $z = \pm\infty$, whereas the solutions should strictly speaking only be trusted where the constant modulus approximation is good, i.e. in the interior of the bubbles given by $|z| < R_c + \sqrt{R_0^2 + \tau^2}$. In practise, this does not matter, since gauge-invariant physical fields only propagate inside the causal future of bubble-wall intersections $I^+(\text{C})$. This region extends beyond the overlap region found by extrapolating the original bubble trajectories (dotted lines in Fig. 3), but never exits the union of the interior of the two bubbles.

The vector potential is chosen to be zero initially, $a(t_c, z) = 0$, and its derivative is determined from Eq. (20). One obtains $\partial_\tau a(t_c, z) = m^2 \theta_0 \text{sgn}(z)/(et_c)$. The solution of the linearised equations (18) and (19) for $\tau > t_c$ then becomes [11]

$$\theta_a(\tau, z) = \frac{\theta_0 t_c}{\pi \tau} \int_{-\infty}^{\infty} \frac{dk}{k} \sin kz \left(\cos \omega(\tau - t_c) + \frac{1}{\omega t_c} \sin \omega(\tau - t_c) \right), \quad (24)$$

$$a(\tau, z) = \frac{\theta_0 m^2 t_c}{\pi e \tau^3} \int_{-\infty}^{\infty} \frac{dk}{k} \sin kz \left[-\frac{\tau - t_c}{\omega^2 t_c} \cos \omega(\tau - t_c) + \left(\frac{\tau}{\omega} + \frac{1}{\omega^3 t_c} \right) \sin \omega(\tau - t_c) \right], \quad (25)$$

where $\omega^2 = k^2 + m^2$. These integrals are highly oscillatory, but can be put in a form that

³A similar approach is adopted in Ref. [10].

greatly facilitates their numerical evaluation. Letting $T = \tau - t_c$ we have

$$\theta_a(\tau, z) = \begin{cases} \theta_0 \frac{t_c}{\tau} \int_0^z du \left(\frac{1}{t_c} J_0(m\sqrt{T^2 - u^2}) - mT \frac{J_1(m\sqrt{T^2 - u^2})}{\sqrt{T^2 - u^2}} \right) & , |z| < \tau - t_c \\ \theta_0 \frac{t_c}{\tau} \text{sgn}(z) \left(\cos mT + \frac{1}{mt_c} \sin mT \right) & , |z| > \tau - t_c . \end{cases} \quad (26)$$

Similarly for the vector potential $A^\alpha = x^\alpha a$ we obtain

$$a(\tau, z) = \theta_0 \frac{m^2}{e} \frac{t_c}{\tau^3} \text{sgn}(z) \left[-\frac{T}{m^2 t_c} \cos mT + \left(\frac{\tau}{m} + \frac{1}{m^3 t_c} \right) \sin mT \right] , \quad |z| > \tau - t_c \quad (27)$$

or, for general z ,

$$a(\tau, z) = \frac{1}{\rho} \int_0^z du B^\varphi(\tau, u) , \quad (28)$$

where $\rho = \sqrt{x^2 + y^2}$ is the distance from the z axis, and the azimuthal Abelian field strength $B^\varphi = F^{z\rho} = \rho \partial_z a$ has the closed-form expression

$$B^\varphi(\tau, z) = \begin{cases} \rho \frac{\theta_0 m^2 t_c}{e \tau^3} \left(\tau J_0(m\sqrt{T^2 - z^2}) + \frac{\sqrt{T^2 - z^2}}{mt_c} J_1(m\sqrt{T^2 - z^2}) \right) & , |z| < \tau - t_c \\ 0 & , |z| > \tau - t_c . \end{cases} \quad (29)$$

The corresponding “electric field” E^z is axial and is given by $E^z = F^{0z} = -t \partial_z a = -(t/\rho) B^\varphi(\tau, z)$. The gauge-invariant phase gradient $D_\mu \theta$ can also be written in closed form; in particular $D_z \theta = \partial_z \theta_a$ is obtained directly from Eq. (26). For $\alpha \in \{0, 1, 2\}$ one finds, using Eqs. (19) and (20),

$$D_\alpha \theta = \begin{cases} x_\alpha z \frac{\theta_0 t_c}{\tau^3} \left(m\tau \frac{J_1(m\sqrt{T^2 - z^2})}{\sqrt{T^2 - z^2}} - \frac{1}{t_c} J_0(m\sqrt{T^2 - z^2}) \right) & , |z| < \tau - t_c \\ 0 & , |z| > \tau - t_c . \end{cases} \quad (30)$$

The physical fields B^φ , E^z , and $D_\mu \theta$ are nonzero only in the causal future of bubble-wall intersections $I^+(C) = \{(z, \tau) \mid |z| < \tau - t_c\}$. In the 3+1 dimensional coordinates at a particular time t this corresponds to a region enclosed by two rotational paraboloids shown as dashed curves in Fig. 3a. The physical fields are generated by sources on the superluminarily expanding circle C_t of most recent intersection ($\rho = \rho_c \equiv \sqrt{t^2 - t_c^2}$, $z = 0$) and propagate towards the z axis, i.e. *into* the bubble overlap region.

One characteristic of the step-function approximation is that the original discontinuity of $2\theta_0$ in the initial condition for the phase splits after the collision into two equal discontinuities of magnitude $\theta_0 t_c/\tau$ at $z = \pm(\tau - t_c)$. Similarly, the Abelian field strength has a discontinuity on $I^0(C)$; the limit from the interior is $B_{|z| \rightarrow (\tau - t_c)_-}^\varphi = \theta_0 m^2 t_c \rho / (e\tau^2)$, while it is zero outside $I^+(C)$.

On the plane $z = 0$ the field strength B^φ oscillates about zero with an amplitude which is an increasing [decreasing] function of ρ [τ]. The largest field strength anywhere is found on the circle C_t of most recent intersection ($\rho = \rho_c$, $z = 0$) and has the value $|B_{\max}| = \theta_0 m^2 \rho_c / (e t_c)$. As this circle expands, $|B_{\max}| \propto t \approx r(t)$ at late times t , where $r(t)$ is the bubble radius. The field strength B^φ around the maximum defines a peak, the radial width of which, $\Delta\rho$, can be estimated from the location of the first zero of $B^\varphi(\tau, 0)$ for $\tau > t_c$ (i.e. $\rho < \rho_c$). With $m(\tau - t_c) = x_0$ at this zero one finds

$$\Delta\rho = \rho_c - \sqrt{t^2 - (t_c + \frac{x_0}{m})^2} \sim \frac{x_0(2mt_c + x_0)}{2m^2 t}, \quad (31)$$

where $x_{01} < x_0 < x_{11}$ and x_{n1} is the smallest positive zero of the Bessel function $J_n(x)$, $x_{01} \approx 2.405$, $x_{11} \approx 3.832$. The last expression in Eq. (31) is the leading behaviour at large times t . The narrowing of the peak with time is a relativistic effect. For a fixed value of τ , the field-strength peak extends in the z direction across $I^+(C)$, so that the width in that direction can be estimated as $\Delta z = x_0/m$.

We can now derive a crude estimate of the Abelian flux contained in the maximal peak by taking

$$\Phi_{B,\text{peak}} \approx |B_{\max}| \Delta\rho \Delta z \sim \frac{\theta_0}{e} x_0^2 \left(1 + \frac{x_0}{2mt_c}\right), \quad (32)$$

where the last expression is the constant flux approached at late times. One can compare this to the total flux of B^φ through a semi-infinite plane based on the z axis (i.e. the total flux of all field lines that “run around the z axis”). This flux, Φ_B , is obtained by evaluating the line integral of A_μ at constant time $t > t_c$ along the path ABDEA indicated in Fig. 3a. In the axial gauge $A_z = 0$, the segments AB and DE do not contribute to the integral. In order to enclose all flux of the Abelian field strength, the segments BD and EA must be chosen so that their z coordinates satisfy $|z| > t - t_c$, and the points D and E must be located at $\rho > \rho_c$ (i.e. $\tau < t_c$). Assuming that the vector potential A_k vanishes for $\tau < t_c$, in accordance with the initial condition, only ρ such that $0 < \rho < \rho_c$ contribute to the integral. From Eq. (27) we find

$$\begin{aligned} \Phi_B(t) &= - \left(\int_{BD} + \int_{EA} \right) dx^\alpha A_\alpha = 2 \int_{t_c}^t d\tau \tau a(\tau, |z|) \\ &= \frac{2\theta_0}{e} \left[1 - \frac{t_c}{t} \left(\cos m(t - t_c) \right) + \frac{1}{mt_c} \sin m(t - t_c) \right], \quad t > t_c. \end{aligned} \quad (33)$$

Note that the integral receives no contributions from regions where the Higgs-field modulus X is fluctuating, and therefore the expression (33) for the total flux is valid also for large initial phase difference $\Delta\theta_0$ of the bubbles (see discussion after Eq. (21)). In this sense, the total flux is of a topological nature.

As a function of time, the Abelian flux Φ_B rises from zero and begins to perform damped oscillations about the late-time limit $\Delta\theta_0/e$, where $\Delta\theta_0 = 2\theta_0$ is the initial phase difference of the two bubbles. The amplitude of these oscillations decreases as t^{-1} . We emphasise that the flux does not go away; it is there to stay.

Comparing with Eq. (32) we see that the flux $\Phi_{B,\text{peak}}$ contained in the maximal peak is of the same order of magnitude as (or somewhat larger than⁴) the total flux Φ_B . This shows that a significant portion of the total flux is contained in an outward travelling circular flux tube near $\rho = \rho_c$, $z = 0$ whose field strength B_{max} is increasing with time.

4 A New, Smooth Analytical Solution

The step-function approximation described in the previous section gives a rough picture of the qualitative behaviour of the physical fields in a U(1) bubble collision. For instance, by looking ahead to Fig. 4 one can see that the shape of the profile of the Abelian field strength in the bubble overlap region is quite well reproduced.

On the other hand, the step-function approximation predicts a peak value of the field strength that differs by a factor of four from the correct value obtained in numerical simulations (a factor of sixteen difference in energy density). Moreover, the solutions (26)–(30) have discontinuities on the future null surface of bubble intersections $I^0(C)$ and are thus unable to account for the behaviour of the fields near that surface. Finally, the solutions are limited to the region $\tau \geq t_c$ (where $\tau = \sqrt{t^2 - \rho^2}$) and therefore provide no clue to the field behaviour shortly before the bubble collisions or, at later times, outside the bubble walls.

Realistic bubble walls of finite width, such as given by Eq. (5), have exponential tails that begin to overlap long before the instant of collision. The overlapping tails initiate the evolution of the phase of the scalar field and of the vector potential so that, in contrast with the assumption made in Sec. 3.1, the functions $\partial_\tau \theta_a$ and $A^\alpha = x^\alpha a$ are already nonzero when the collision reaches full impact at $\tau = t_c$.

In this section, we shall model the initial evolution of θ_a and a and obtain a smooth analytical solution. To do so, we first observe that the scalar Higgs field of two well-separated bubbles can be written [10, 13]

$$\Phi(x) = \Phi_1(x) + \Phi_2(x) , \tag{34}$$

⁴This is not a contradiction, because B^φ changes sign in the bubble overlap region

where Φ_1, Φ_2 are $O(1,3)$ -symmetric solutions of the Higgs field equation with $\Phi_i \rightarrow 0$ away from the bubbles and $|\Phi_i|$ approaching the vacuum expectation value η well inside each bubble. In the absence of gauge fields the linear superposition (34) remains a good approximation even when the bubbles begin to overlap, because in the region of overlap the Higgs field is small and the field equation can be linearised about $\Phi = 0$. When gauge fields are included, the reliability of the linear superposition approximation for describing the phase of the Higgs field depends on the choice of gauge. We have found that in the *temporal gauge* the initial evolution of the phase is well described by a linear superposition approximation, as long as the bubble overlap is weak.

The position of a bubble wall can be defined as the set of points where $|\Phi_i| = \eta/2$, $i = 1, 2$. Note that this definition gives the location of each bubble wall in the absence of the other bubble. The bubble collision is then defined as an event x for which $|\Phi_1(x)| = |\Phi_2(x)| = \eta/2$. This corresponds to the intersection of the extrapolated trajectories of two well-separated bubble walls. When the bubbles begin to overlap strongly, the actual scalar field $\Phi(x)$ has a nonlinear behaviour and therefore cannot be used to define the event of collision.

Using the same geometry as in Sec. 3, depicted in Fig. 3, the assumptions underlying the present analytical treatment can be formulated as follows: The bubble collision occurs at $\tau = t_c$, $z = 0$ with $\tau = \sqrt{t^2 - \rho^2}$. For $\tau \leq t_c$ the field evolution is given by the linear superposition (34). This defines the fields outside the bubble walls as well as before the time of collision. For $\tau > t_c$ the scalar field is assumed to have constant modulus $|\Phi| = \eta$. This reduces the problem to one of finding the solution of the linearised equations (18) and (19) with initial conditions at $\tau = t_c$ provided by the linear superposition.

Note that although linear superposition is an excellent approximation for $\tau \ll t_c$, and the constant-modulus approximation works very well for $\tau \gg t_c$, both approximations break down near $\tau = t_c$. The approach taken here is therefore one of joining two asymptotic solutions across a non-linear region where no solutions are known.

Some further approximations are necessary. We assume that the thin-wall approximation (12) is valid. Moreover, we shall require that the two bubbles overlap negligibly at the time of their nucleation, $t = 0$. At this time, the bubble walls are a distance $2(R_c - R_0)$ apart, and the thickness of the bubble wall is given by μ_0^{-1} (refer to Eqs. (7) and (11)). One obtains the *no-overlap condition*

$$2\mu_0(R_c - R_0) \gg 1. \quad (35)$$

Because of the exponential decay of the bubble-wall profile, results accurate to about 3% are obtained already when the left-hand side of Eq. (35) is greater than 3.5. Via the identity $t_c^2 = R_c^2 - R_0^2$ the condition of no overlap also implies the following very useful

relation,

$$2\beta \equiv \frac{R_c}{2\mu_c t_c^2} \ll 1 . \quad (36)$$

Let us now consider two bubbles, one with constant Higgs phase θ_0 centred at $x = y = 0$, $z = R_c$ and the other with constant Higgs phase $-\theta_0$ centred at $x = y = 0$, $z = -R_c$. It is convenient to express the Higgs modulus in the bubbles as a product of the vacuum expectation value η and a function f of the variables

$$u_{\pm} = \frac{R_0^2 - (z \mp R_c)^2 + \tau^2}{2R_c} , \quad (37)$$

which possess $O(1,3)$ symmetry with respect to the nucleation events $(0, 0, 0, \pm R_c)$, respectively. The modulus of the Higgs field in each bubble is then

$$\eta f(u_{\pm}) = \phi_b(\sqrt{x^2 + y^2 + (z \mp R_c)^2 - t^2}) = \phi_b(\sqrt{R_0^2 - 2R_c u_{\pm}}) , \quad (38)$$

where ϕ_b is the approximate bounce solution given by Eq. (5) or, alternatively, Eq. (6). The positions of the bubble walls correspond to $u_{\pm} = 0$. The profile function $f(u_{\pm})$ has non-negligible variation only near the bubble walls or, more precisely, for $|u_{\pm}| \lesssim \mu_c^{-1}$, where $\mu_c^{-1} = R_0/(\mu_0 R_c)$ is the width of the bubble wall at the collision time t_c given by equation (11). Using the thin-wall condition (12) it is easy to show that $\mu_c^{-1} \ll R_0^2/(2R_c)$. The argument of the bounce profile, Eq. (38), can therefore be safely linearised, giving

$$\eta f(u_{\pm}) \approx \phi_b(R_0 - R_c u_{\pm}/R_0) . \quad (39)$$

The linear superposition (34) can now be written

$$\Phi(x) = X(x)e^{i\theta_t(x)} = \eta \left[f(u_+)e^{i\theta_0} + f(u_-)e^{-i\theta_0} \right] . \quad (40)$$

We obtain the following expressions, which are assumed to be valid for $\tau \leq t_c$:

$$X^2 = \eta^2 \left\{ [f(u_+) + f(u_-)]^2 \cos^2 \theta_0 + [f(u_+) - f(u_-)]^2 \sin^2 \theta_0 \right\} , \quad (41)$$

$$\theta_t = \arctan \left[\tan \theta_0 \frac{f(u_+) - f(u_-)}{f(u_+) + f(u_-)} \right] , \quad (42)$$

$$\partial_{\tau} \theta_t = \sin 2\theta_0 \frac{\tau}{R_c} \frac{\eta^2}{X^2} [f'(u_+)f(u_-) - f'(u_-)f(u_+)] , \quad (43)$$

$$\partial_z \theta_t = \sin 2\theta_0 \frac{\eta^2}{X^2} \left[\left(1 - \frac{z}{R_c}\right) f'(u_+)f(u_-) + \left(1 + \frac{z}{R_c}\right) f'(u_-)f(u_+) \right] , \quad (44)$$

where θ_t is the phase of the Higgs field in the temporal gauge.

At the collision the argument u_{\pm} simplifies to

$$u_{\pm} = \pm z \left(1 \mp \frac{z}{2R_c} \right) , \quad \tau = t_c . \quad (45)$$

We see that u_{\pm} is zero not only in the plane of collision $z = 0$ but also on the two remote bubble walls located at $z = \pm 2R_c$. However, no interesting dynamics takes place near the remote bubble walls, and we can ignore their presence. This is because physical fields excited by the collision can extend at most a distance $\sim \mu_c^{-1}$ outside the null surface $I^0(C)$ drawn in Fig. 3. The protrusion beyond the ideal null surface is due to the finite thickness of the bubble wall. It can be shown that the distance between $I^0(C)$ and the remote wall remains always larger than $R_c + t_c$. Therefore, because of the no-overlap condition (35) and the thin-wall condition (12), physically interesting fields will never reach the remote bubble walls.

Concentrating instead on the collision region near $z = 0$, we notice that, for $\tau = t_c$, the profile function $f(u_{\pm})$ has non-negligible variation only for $|z| \lesssim \mu_c^{-1}$ and quickly approaches a constant value for larger $|z|$. From Eq. (35) we find that $\mu_c^{-1} \ll 2R_c$ and we can thus ignore the term of order z/R_c in Eq. (45), obtaining

$$u_{\pm} \approx \pm z, \quad \tau = t_c. \quad (46)$$

Similarly, for $\tau \leq t_c$ the products $f'(u_{\pm})f(u_{\mp})$ in Eq. (44) are non-zero only for $|z| \lesssim \mu_c^{-1}$, and we can neglect the term z/R_c also in this equation, which reduces to

$$\partial_z \theta_t = \sin 2\theta_0 \frac{\eta^2}{X^2} [f'(u_+)f(u_-) + f'(u_-)f(u_+)] , \quad \tau \leq t_c. \quad (47)$$

4.1 Solution for the Abelian Field Strength

In this section, we show that the initial evolution of the scalar Higgs field in the linear superposition approximation generates non-zero vector fields already before the collision time t_c from the exponential tails preceeding the expanding bubble walls. The vector field is evolved to $\tau = t_c$, and its values there are used as initial conditions for the ensuing linear evolution.

For non-constant Higgs modulus X , the z component of the Maxwell field equation, Eq. (20), generalises to

$$\partial_z(3a + \tau \partial_{\tau} a) = 2eX^2 \partial_z \theta_a, \quad (48)$$

where θ_a is the phase of the Higgs field in the axial gauge defined by $A^3 = 0$. This phase can be expressed in terms of θ_t , the phase in the temporal gauge defined by $A^0 = 0$, as follows

$$\theta_a = \theta_t - \frac{e}{2} \int_{-\infty}^{\tau^2} a d(\tau^2), \quad (49)$$

where we used the initial condition that $A^{\mu} \rightarrow 0$ and therefore $\theta_a - \theta_t \rightarrow 0$ as $\tau^2 = t^2 - \rho^2 \rightarrow -\infty$. One obtains the differential-integral equation

$$\partial_z(3a + \tau \partial_{\tau} a) = 2eX^2 \left(\partial_z \theta_t - \frac{e}{2} \int_{-\infty}^{\tau^2} \partial_z a d(\tau^2) \right). \quad (50)$$

We shall show at the end of this section that the integral term on the right-hand side of this equation is subdominant and can be neglected provided that

$$\beta^2 m^2 t_c^2 \cos^2 \theta_0 \frac{\pi^2}{12} \ll 1 . \quad (51)$$

Using Eq. (47) the equation for a then becomes

$$\partial_\tau(\tau^3 \partial_z a) = \frac{m^2}{e} \sin 2\theta_0 \tau \partial_\tau [f(u_+) f(u_-)] . \quad (52)$$

We now specialise to the approximation of the bounce solution given by Eq. (6). Using Eq. (39) one obtains

$$f(u) = \frac{1}{2} [1 + \tanh(2\mu_c u)] . \quad (53)$$

Equation (52) can then be integrated provided that we make another well founded approximation. Realising that the composite function $(f \circ u)(\tau)$ is monotonically increasing for all z , we have for $\tau \leq t_c$ the leading behaviour $f(u) \sim g(z) \exp[4\mu_c t_c (\tau - t_c)/R_c]$ for some function $g(z)$. The right-hand side of Eq. (52) consequently has the leading behaviour $\sim h(z) \tau^2 \exp[8\mu_c t_c (\tau - t_c)/R_c]$ for some function $h(z)$. Its integral with respect to τ is thus dominated by contributions from an interval $t_c - \delta \lesssim \tau \leq t_c$, where $\delta = R_c/(8\mu_c t_c) = \beta t_c/2 \ll t_c$. Let us now consider the identity $\tau^2 = t_c^2 + 2t_c(\tau - t_c)[1 + (\tau - t_c)/(2t_c)]$. Near $\tau = t_c$ we can replace τ^2 by its linear expansion, provided that $|\tau - t_c|/(2t_c) \ll 1$. However, the latter condition is always satisfied in the interval $(t_c - \delta, t_c]$ by virtue of Eq. (36). We can therefore consistently replace the variables u_\pm by new variables v_\pm , linear in τ , defined by

$$v_\pm = \pm z + \frac{t_c}{R_c}(\tau - t_c) . \quad (54)$$

A term $-z^2/(2R_c)$ was omitted from v_\pm in analogy with the discussion leading to Eq. (46). To justify this, let us again ignore the remote bubble walls located at $z = \pm(R_c + \sqrt{R_c^2 + \tau^2 - t_c^2})$ and take into account that $f(v_\pm)$ has non-negligible variation only for $|v_\pm| \lesssim \mu_c^{-1}$. It then follows from the triangle inequality and Eq. (35) that $|z| \leq |v_\pm| + t_c |\tau - t_c|/R_c \lesssim 9\mu_c^{-1}/8 \ll 2R_c$ in the interval $t_c - \delta < \tau \leq t_c$.

The linearisation (54) has the added benefit that $f(v_\pm)$ has an exponential fall-off as $\tau \rightarrow -\infty$ (in contrast, $f(u_\pm)$ approaches unity as $\tau \rightarrow -\infty$ and falls off exponentially only for $\tau^2 \rightarrow -\infty$). Because the contribution from $\tau \ll t_c - \delta$ is negligible, for the purpose of integration we can extend the domain of definition of the fields to $\tau \in (-\infty, t_c]$, identifying only positive τ with the physical quantity $\sqrt{t^2 - \rho^2}$.

By means of integration by parts, and using the initial condition $a(\tau \rightarrow -\infty, z) = 0$, the solution of Eq. (52) is written

$$\begin{aligned}\partial_z a &= \frac{m^2 R_c}{e \tau^3} \sin 2\theta_0 \left\{ \tau f(v_+) f(v_-) - \int_{-\infty}^{\tau} f(v_+) f(v_-) d\tau \right\} \\ &= \frac{m^2 R_c}{e 4\tau^3} \sin 2\theta_0 \left\{ \tau (1 + \tanh 2\mu_c v_+) (1 + \tanh 2\mu_c v_-) \right. \\ &\quad \left. - 2\beta t_c [\ln(1 + e^{4\mu_c v_+}) + \ln(1 + e^{4\mu_c v_-})] \right. \\ &\quad \left. + 2\beta t_c [\ln(1 + e^{4\mu_c v_+}) - \ln(1 + e^{4\mu_c v_-})] \coth 4\mu_c z \right\},\end{aligned}\quad (55)$$

where β is defined in Eq. (36). The expression for $\partial_z a$ can be integrated, using the condition $a(\tau, 0) = 0$ prescribed by symmetry. One obtains

$$\begin{aligned}a(\tau, z) &= \beta \frac{t_c^2 m^2}{\tau^3 e} \sin 2\theta_0 \left\{ \frac{\tau b^2}{b^2 - 1} \ln \frac{1 + bc}{b + c} \right. \\ &\quad \left. + \frac{1}{2} \beta t_c \left[\ln(c) \ln(1 - b^2) + \text{Li}_2 \left(-\frac{b(1 + c)}{c(1 - b)} \right) + \text{Li}_2 \left(\frac{b(c - 1)}{c(1 + b)} \right) - 2 \text{Li}_2 \left(-\frac{b}{c} \right) \right. \right. \\ &\quad \left. \left. - \text{Li}_2 \left(-\frac{b(1 + c)}{1 - b} \right) - \text{Li}_2 \left(\frac{b(1 - c)}{1 + b} \right) + 2 \text{Li}_2(-bc) \right] \right\},\end{aligned}\quad (56)$$

where

$$b = \exp \left[4\mu_c \frac{t_c}{R_c} (\tau - t_c) \right], \quad c = \exp(4\mu_c z), \quad (57)$$

and where the poly-logarithm function $\text{Li}_n(z)$ is defined by [27, 28]

$$\text{Li}_n(z) = \frac{(-1)^n}{(n - 1)!} \int_0^1 dx \frac{\ln^{n-1} x}{x - 1/z} = \sum_{k=1}^{\infty} \frac{z^k}{k^n}. \quad (58)$$

For real z and $n = 2$ the power series is convergent for $|z| \leq 1$. The evaluation of $\text{Li}_2(z)$ for z near or outside the convergence radius of the series is discussed in Appendix B.

The expressions (55) and (56) are valid for $t_c - \delta \lesssim \tau \leq t_c$ and approach zero rapidly for $\tau < t_c - \delta$. Nevertheless, these expressions for $\partial_z a$ and a have poles at $\tau = 0$. The poles are an artifact of the linearisation (54) and would cancel in the exact solutions, leading to finite (and exponentially small) functional values of a and $\partial_z a$ as $\tau \rightarrow 0$. Because $\delta \ll t_c$ one can easily remedy this slight problem by explicitly setting $a(\tau, z) \equiv 0$ for $\tau \ll t_c - \delta$.

As the next step, we shall now find expressions for $a(t_c, z)$ and $\partial_\tau a(t_c, z)$ to use as initial conditions for the linear equations governing the evolution for $\tau > t_c$. Taking the limit $\tau \rightarrow t_c$ in Eq. (56), using the asymptotic result (B.5) for the dilogarithm $\text{Li}_2(x)$

(see Appendix B) as well as the relations (B.4) and (B.3), we find

$$a(t_c, z) = \beta \frac{m^2 \sin 2\theta_0}{e} \frac{1}{2} \left\{ \tanh 2\mu_c z + \beta \left[8\mu_c z \ln(2 \cosh 2\mu_c z) \right. \right. \\ \left. \left. + \text{Li}_2(\tanh 2\mu_c z) - \text{Li}_2(-\tanh 2\mu_c z) + 2 \text{Li}_2(-e^{4\mu_c z}) - 2 \text{Li}_2(-e^{-4\mu_c z}) \right] \right\} \quad (59)$$

$$\approx \beta \left(1 - \beta \frac{\pi^2}{12} \right) \frac{m^2 \sin 2\theta_0}{e} \frac{1}{2} \tanh 2\mu_c z. \quad (60)$$

The expression (60) is an excellent approximation; it was obtained by matching the functions in the limit of large $|z|$ using Eq. (B.5) and the special values $\text{Li}_2(0) = 0$, $\text{Li}_2(-1) = -\pi^2/12$ and $\text{Li}_2(1) = \pi^2/6$.

Similarly, by differentiating Eq. (56) with respect to τ and taking the limit $\tau \rightarrow t_c$, we obtain

$$\begin{aligned} \partial_\tau a(t_c, z) &= -\frac{3}{t_c} a(t_c, z) + \frac{m^2 \sin 2\theta_0}{et_c} \frac{1}{2} \tanh 2\mu_c z \\ &\approx \left(1 - 3\beta + \frac{\pi^2}{4} \beta^2 \right) \frac{m^2 \sin 2\theta_0}{et_c} \frac{1}{2} \tanh 2\mu_c z. \end{aligned} \quad (61)$$

Note that, in the limit of an infinitely steep bubble wall ($\mu_c \rightarrow \infty$, $\beta \rightarrow 0$) and for small Higgs phase difference $2\theta_0$, Eqs. (59) and (61) reduce to the initial conditions $a(t_c, z) = 0$, $\partial_\tau a(t_c, z) = m^2 \theta_0 \text{sgn}(z)/(et_c)$ of the Kibble-Vilenkin step function approximation (see Sec. 3.1 and Ref. [11]).

The solution of Eq. (19) for $\tau \geq t_c$ subject to the initial conditions (60) and (61) is expressed as

$$\begin{aligned} a(\tau, z) &= \frac{m^2 \sin 2\theta_0}{e} \frac{t_c}{8\mu_c} \frac{1}{\tau^3} \int_{-\infty}^{\infty} dk \frac{\sin kz}{\sinh \frac{\pi k}{4\mu_c}} \left\{ \left[-\frac{\tau - t_c}{\omega^2 t_c} + \beta \left(1 - \beta \frac{\pi^2}{12} \right) t_c \tau \right] \cos \omega(\tau - t_c) \right. \\ &\quad \left. + \left[\frac{\tau}{\omega} + \frac{1}{\omega^3 t_c} - \beta \left(1 - \beta \frac{\pi^2}{12} \right) \frac{t_c}{\omega} \right] \sin \omega(\tau - t_c) \right\}, \end{aligned} \quad (62)$$

where $\omega^2 = m^2 + k^2$. We have retained as many orders of the small parameter β as is necessary to ensure that this solution joins smoothly with the solution for $\tau \leq t_c$ given in Eq. (56).

The Abelian field strength is defined by $B^\varphi = \rho \partial_z a$, where $\rho = \sqrt{x^2 + y^2}$ and where $\partial_z a(\tau, z)$ is given by Eq. (55) for $\tau \leq t_c$, or obtained for $\tau \geq t_c$ by differentiating Eq. (62).

4.2 Solution for the Gauge-Invariant Phase

Let us now turn to the gauge-invariant phase $\tilde{\theta}$. Because of Eq. (23) it is identical to the phase θ_a in the axial gauge defined by $A^3 = 0$. The phase θ_a is given by Eq. (49) which

has two terms, one being the phase θ_t in the temporal gauge and the other an integral of the vector-potential field $a(\tau, z)$. For $\tau \leq t_c$, these can be evaluated using the linear superposition approximation.

The phase θ_t is given explicitly by Eq. (42). For $\tau < t_c$ we shall therefore use the more complicated, but precise, expressions for the bubble profile function with $f(u)$ given by Eq. (38) and ϕ_b given by Eq. (5). This bounce solution ϕ_b has the correct exponential tail far from the bubble wall, which is particularly important for the global behaviour of gauge-invariant phase $\tilde{\theta}$.

The integral in Eq. (49) can be evaluated using the expression for $a(\tau, z)$ given in Eq. (56), provided that one expands inverse powers of τ in a Taylor series about $\tau = t_c$. It suffices to do the calculation to lowest order in the parameter β . One finds

$$\begin{aligned}
e \int_{-\infty}^{\tau} d\tau \tau a &= \beta^2 m^2 t_c^2 \frac{\sin 2\theta_0}{2} \times \\
&\times \left\{ \frac{1}{2} \ln \frac{b+c}{1+bc} \ln \left(\frac{(1+bc) \left(1 + \frac{b}{c}\right) \left(\sqrt{c} + \frac{1}{\sqrt{c}}\right)^2}{(1-b^2)^2} \right) + \ln c \ln \left(\frac{(1+bc) \left(1 + \frac{b}{c}\right)}{\sqrt{c} + \frac{1}{\sqrt{c}}} \right) \right. \\
&+ \text{Li}_2(1-c) - \text{Li}_2\left(\frac{c-1}{c}\right) - \text{Li}_2\left(\frac{1}{1+c}\right) + \text{Li}_2\left(\frac{c}{1+c}\right) \\
&\left. + \text{Li}_2\left(\frac{c-1}{b+c}\right) - \text{Li}_2\left(\frac{b+c}{1+c}\right) - \text{Li}_2\left(\frac{1-c}{1+bc}\right) + \text{Li}_2\left(\frac{1+bc}{1+c}\right) \right\}, \quad (63)
\end{aligned}$$

which is valid for $\tau \leq t_c$. In particular, at $\tau = t_c$ the expression reduces to

$$\begin{aligned}
e \int_{-\infty}^{t_c} d\tau \tau a &= \beta^2 m^2 t_c^2 \frac{\sin 2\theta_0}{2} \left\{ 4\mu_c z \ln(2 \cosh 2\mu_c z) + \text{Li}_2(\tanh 2\mu_c z) - \text{Li}_2(-\tanh 2\mu_c z) \right. \\
&+ \text{Li}_2(1 - e^{4\mu_c z}) - \text{Li}_2(1 - e^{-4\mu_c z}) - \text{Li}_2\left(\frac{1}{1 + e^{4\mu_c z}}\right) + \text{Li}_2\left(\frac{1}{1 + e^{-4\mu_c z}}\right) \left. \right\} \\
&\approx \beta^2 m^2 t_c^2 \frac{\sin 2\theta_0}{2} \frac{\pi^2}{12} \tanh 2\mu_c z. \quad (64)
\end{aligned}$$

We are now ready to derive approximative expressions for $\theta_a(t_c, z)$ and $\partial_\tau \theta_a(t_c, z)$ to be used as initial conditions for the ensuing linear evolution. First, from Eqs. (42) and (46) we obtain

$$\begin{aligned}
\theta_t(t_c, z) &= \arctan \left[\tan \theta_0 \frac{f(z) - f(-z)}{f(z) + f(-z)} \right] \\
&\approx \arctan(\tan \theta_0 \tanh 2\mu_c z) \approx \theta_0 \tanh \left[\frac{\tan \theta_0}{\theta_0} 2\mu_c z \right], \quad (65)
\end{aligned}$$

where we used Eq. (53) in the intermediate step. Substituting this result together with

Eq. (64) into Eq. (49) we find the initial condition

$$\theta_a(t_c, z) \approx \theta_0 \tanh \left[\frac{\tan \theta_0}{\theta_0} 2\mu_c z \right] - \beta^2 m^2 t_c^2 \frac{\sin 2\theta_0}{2} \frac{\pi^2}{12} \tanh 2\mu_c z . \quad (66)$$

Turning next to the τ derivative given by Eq. (43), using Eqs. (46) and (53) we have that

$$\partial_\tau \theta_t(t_c, z) = -\frac{2\mu_c t_c}{R_c} \tan \theta_0 g(\mu_c z) , \quad (67)$$

where the function $g(x)$ is defined by

$$g(x) = \frac{\tanh 2x}{\cosh^2 2x + \tan^2 \theta_0 \sinh^2 2x} . \quad (68)$$

We shall need an approximation of the function g which possesses a simple Fourier transform. To this effect, let us define the value x_0 by

$$x_0 = \frac{1}{4} \cosh^{-1} \left[\frac{1}{2} (1 + \sqrt{5 + 4 \cos 2\theta_0}) \right] \quad (69)$$

satisfying

$$g(x_0) = 4 \left(\frac{\sqrt{5 + 4 \cos 2\theta_0} - 1}{\sqrt{5 + 4 \cos 2\theta_0} + 3} \right)^{\frac{1}{2}} \frac{\cos^2 \theta_0}{\sqrt{5 + 4 \cos 2\theta_0} + 1 + 2 \cos 2\theta_0} \quad (70)$$

An excellent approximation to $g(x)$ is then given by

$$g(x) \approx 16 x_0^3 g(x_0) \frac{x}{(3x_0^2 + x^2)^2} . \quad (71)$$

Combining Eqs. (67), (71), (60) and (49) one finds the other initial condition

$$\begin{aligned} \partial_\tau \theta_a(t_c, z) &\equiv \partial_\tau \theta_t(t_c, z) - e t_c a(t_c, z) \\ &\approx -\frac{32\mu_c t_c}{R_c} \tan \theta_0 \frac{x_0^3 g(x_0) \mu_c z}{(3x_0^2 + \mu_c^2 z^2)^2} - \beta \left(1 - \beta \frac{\pi^2}{12} \right) m^2 t_c \frac{\sin 2\theta_0}{2} \tanh 2\mu_c z . \end{aligned} \quad (72)$$

The solution of Eq. (18) for $\tau \geq t_c$ subject to the initial conditions (66) and (72) is given by

$$\begin{aligned} \theta_a(\tau, z) &= \frac{t_c}{\tau} \int_{-\infty}^{\infty} dk \frac{\sin kz}{4\mu_c} \times \\ &\left\{ \left[\frac{\theta_0^2}{\tan \theta_0 \sinh \left(\frac{\theta_0}{\tan \theta_0} \frac{\pi k}{4\mu_c} \right)} - \frac{\sin 2\theta_0}{2} \frac{\beta^2 \pi^2 m^2 t_c^2}{12 \sinh \left(\frac{\pi k}{4\mu_c} \right)} \right] \cos \omega(\tau - t_c) \right. \\ &+ \left[\frac{\theta_0^2}{\tan \theta_0 \sinh \left(\frac{\theta_0}{\tan \theta_0} \frac{\pi k}{4\mu_c} \right)} - \frac{\sin 2\theta_0}{2} \frac{\beta m^2 t_c^2}{\sinh \left(\frac{\pi k}{4\mu_c} \right)} \right. \\ &\left. \left. - \tan \theta_0 \frac{32 t_c^2}{\sqrt{3} R_c} g(x_0) x_0^2 k \exp(-\sqrt{3} x_0 |k| / \mu_c) \right] \frac{\sin \omega(\tau - t_c)}{\omega t_c} \right\} , \end{aligned} \quad (73)$$

where $\omega^2 = m^2 + k^2$.

Finally, let us justify the approximation made in Eq. (50), where the integral term was neglected. To estimate the relative significance of the two terms in the right-hand side of that equation, recall that the integral $\int d\tau \tau \partial_z a$ is an increasing function of τ which is significantly nonzero only in a narrow interval $t_c - \delta \lesssim \tau \leq t_c$, where $\delta = R_c/(8\mu_c t_c) = \beta t_c/2 \ll t_c$. The largest values of the integral occur at $\tau = t_c$, where it is easily compared to the other term. From Eq. (64) one obtains

$$e \int_{-\infty}^{t_c} d\tau \tau \partial_z a \approx \beta^2 m^2 t_c^2 \mu_c \sin 2\theta_0 \frac{\pi^2}{12} \text{sech}^2 2\mu_c z, \quad (74)$$

and from Eq. (65), similarly,

$$\partial_z \theta_t(t_c, z) \approx 2\mu_c \tan \theta_0 \text{sech}^2 \left(\frac{\tan \theta_0}{\theta_0} 2\mu_c z \right). \quad (75)$$

Therefore, the condition for the integral in Eq. (50) to be negligible is given by Eq. (51).

5 Lattice Computation

In order to compare our approximate analytical solutions to the true evolution of fields in the original field theory, we have evolved the system of two bubbles numerically on the lattice, using the temporal gauge $A^0 = 0$ and the techniques described in Appendix A. As the first step of such a lattice simulation it is necessary to specify the initial conditions. In particular, one must determine the initial shape of the bubble walls.

For definiteness we consider the Higgs potential (1) with the fields and coordinates rescaled so that $\lambda = \eta = 1$. We choose $\epsilon = 0.2$, corresponding to the thin-wall condition (12) being marginally satisfied. This means that the bubble wall is thin, but not extremely thin, compared to the nucleation radius R_0 (see Fig. 1). The gauge coupling of the rescaled fields is taken to be $e = 0.5$.

The Euclidean field equation relevant to the nucleation of a single spherical bubble at rest, Eq. (3), has been solved using a shooting method. At $t = 0$ in Minkowski space the spatial dependence of the single-bubble configuration coincides with that of the Euclidean instanton solution. The initial two-bubble configuration is approximated by the linear superposition of the scalar fields of two well separated single bubbles. The vector potential A^i and the time derivatives of all fields are set to zero initially.

We have used a spatial Cartesian grid consisting of 125^3 unit cells with a lattice spacing of $a = 0.2$ (this a need not be confused with the field $a(\tau, z)$ defined in Eq. (17)). In order to maximise the dynamical range, we placed the bubbles in two adjacent corners of our box and employed reflective boundary conditions. More precisely, on each face

of the box we imposed $\partial\Phi/\partial x^\perp = 0$, $A^\perp = 0$, and $\partial A^\parallel/\partial x^\perp = 0$, where \perp signifies the outward normal and A^\parallel denotes the two vector-potential components parallel to the face. Derivatives were approximated by symmetric differences, which caused the planes of symmetry in each direction to be located at the lattice points with indices 2 and 124. Thus, the distance between bubble centres is $2R_c = 122a = 24.4$.

Finally, the system was evolved using a time step of ha with $h = 0.2$. The lattice Gauss constraint, Eq. (A.18), was monitored and found to remain zero at the level of machine accuracy, i.e., one part in 10^{15} .

6 Analysis

We shall here present results for the Abelian field strength B^φ and the gauge-invariant Higgs phase $\tilde{\theta} = \int dx^\mu D_\mu \theta$ in the collision of two expanding bubbles. Analytical results, within the Kibble-Vilenkin step-function approximation as well as our new approach, are compared to the true field evolution obtained from the numerical simulation on the lattice.

First, let us review the values of various parameters that occur in the solutions. As was mentioned in the last section, we take $\lambda = \eta = 1$ and $\epsilon = 0.2$ as parameters of the Higgs potential. The gauge coupling is $e = 0.5$ and the bubble radius at the time of collision is $R_c = 12.2$. We then find directly the vector-boson mass $m = \sqrt{2}e\eta = 0.7071$. Expressions (7) and (10) determine, within the thin-wall approximation, the initial bubble-wall slope $\mu_0 = 0.375$ and the nucleation radius $R_0 = 7.5$. The time of collision is obtained from Eq. (15) with $R_i = R_0$, which gives $t_c = \sqrt{R_c^2 - R_0^2} = 9.62$. The bubble-wall slope at the time of collision $\mu_c = \mu_0 R_c / R_0 = 0.61$ is found from Eq. (11). As a consequence, $\beta \equiv R_c / (4\mu_c t_c^2) = 0.054 \ll 1$ as required. Finally, the constant s_0 occurring in Eq. (5) is given by $s_0 = 6.95$. This completes a list of parameters that are uniquely determined by the physical model and by the chosen distance between nucleation centres, $2R_c$. The average value of this bubble separation can also be calculated from the model parameters [31].

The remaining parameter, θ_0 , is determined by the random nature of spontaneous symmetry breaking. We choose $\theta_0 = \pi/8$, corresponding to a particular case in which two colliding bubbles have a Higgs phase difference of $\pi/4$. This phase difference is sufficiently small that important approximations remain valid, such as the assumed constancy of the Higgs-field modulus inside the bubble overlap region after collision. Moreover, it can be checked that the no-overlap condition (35) is satisfied with the left-hand side being approximately 3.5; this ensures that the overlap of two bubbles is negligible at the time of nucleation $t = 0$. Finally, the condition (51), used in the derivation of the analytical solution for $\tilde{\theta}$, is satisfied with the left-hand side being approximately $0.095 \ll 1$. With

the chosen value of θ_0 , Eqs. (69) and (70) give $x_0 = 0.314$ and $g(x_0) = 0.365$.

The results for the Abelian field strength are most easily explained with the help of Fig. 4. The first and third columns of this figure depict results from the numerical evolution of the fields on a lattice, which was described in Sec. 5. Because of the cylindrical symmetry, the fields depend only on the coordinate z along the symmetry axis and the distance ρ from this axis. Two bubbles were initially nucleated in the far left and near corners, defined by $\rho = 0$, $z = \pm 12.2$, with nucleation radius $R_0 = 7.5$. In column (a) we can follow the evolution of the modulus of the scalar field as the bubbles expand. The bubbles first collide at time $t_c = 9.62$, which falls between the first and second frames. As they continue to expand, the modulus within the region of overlap of the two bubbles begins to fluctuate. The fluctuations are moderate, and therefore the approximation of the Higgs modulus by a constant value $|\Phi| = \eta$ within the union of interior of the two bubbles is well justified. A larger distance $2R_c$ between nucleation centres would lead to higher bubble-wall speed at collision, $v_c = \sqrt{1 - R_0^2/R_c^2}$, and therefore to larger fluctuations in the Higgs modulus. Violent fluctuations in the modulus are induced for large phase differences $\Delta\theta_0 \gtrsim \pi/2$ regardless of the collision speed. Therefore, we don't expect our analytical treatment to remain valid for large values of θ_0 .

Turning next to the field strength B^φ depicted in column (c), we notice that the flux of B^φ is mainly concentrated in a peak which moves away from the z axis in the symmetry plane $z = 0$. Because of the cylindrical symmetry, the peak corresponds to a circular flux tube enclosing the region of bubble intersection. In fact, by comparing with column (a), we see that the peak is located near the value of ρ at which the bubbles have most recently come into contact. This circle of most recent intersection is represented by the point C_t in Fig. 3a and has radius $\rho_c = \sqrt{t^2 - t_c^2}$. As a consequence, the flux tube moves away from the symmetry axis with a speed greater than the speed of light. This is not in contradiction with special relativity; the field strength in the peak has been generated locally and causally by the most recent bubble-wall intersection, while the tail toward the bubble interior consists of fields generated by earlier intersections occurring at smaller radius ρ .

In column (b) we observe that the solution obtained by Kibble and Vilenkin using a step-function approximation (see Sec. 3.1 and Ref. [11]) gives a very reasonable qualitative description of the behaviour of the field strength in the region $I^+(C)_t = \{(z, \rho) \mid (t_c + |z|)^2 + \rho^2 < t^2\}$, which constitutes the causal future of bubble intersections and is shown in Fig. 3a. On the other hand, the peak value of the field strength in this approximation is about four times higher than the true peak value obtained from the lattice evolution. The reason for the higher field strength is that the step-function initial condition leads to a much higher time derivative of the field strength at the collision than does the smooth initial condition (61) obtained with finite-width bubble walls.

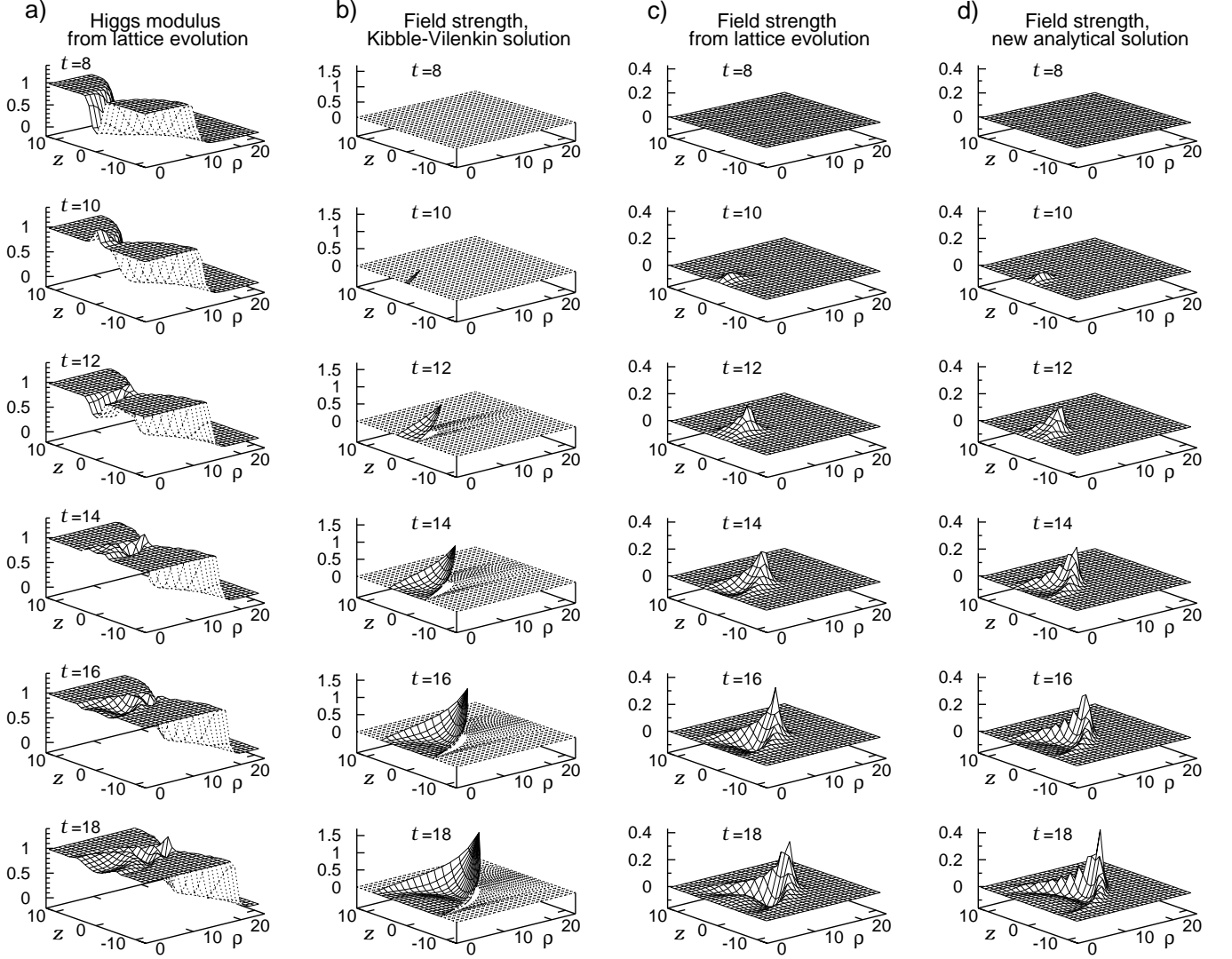


Figure 4: Bubble collision with initial Higgs-field phase difference $\Delta\theta_0 = 2\theta_0 = \pi/4$. a) Lattice evolution of the modulus $|\Phi|$ of the Higgs field, b) Kibble-Vilenkin approximate solution for the azimuthal field strength B^φ , c) Lattice evolution of B^φ , d) Our new analytical solution for B^φ . Here $\rho = (x^2 + y^2)^{1/2}$ is the distance from the symmetry axis of the collision, $|\Phi|$ is measured in units of η , B^φ in units of m^2/e , and ρ, z, t in units of $\lambda^{-1/2}\eta^{-1}$. The centres of the two bubbles are at $\rho = 0, z = \pm 12.2$. The bubbles first collide at time $t_c = 9.62$, which falls between the first and second frames in each column.

The new, smooth analytical solution is displayed in column (d). It is found to be

in excellent agreement with the lattice results (c).⁵ The two solutions are more easily compared in Fig. 5, which shows the field strength on the symmetry plane $z = 0$. Here the agreement of the new solution with the numerical results is rather remarkable. The tail that leads down from the peak towards higher values of ρ is accurately reproduced. We find that the maximum field strength increases with time, and the width of the peak $\Delta\rho$ decreases with time as predicted by the analysis in Sec. 3.1. Note that there is a trough with negative values of the field strength trailing the primary peak by about a peak width. This trough corresponds to an expanding circular flux-tube loop with smaller radius than the primary one and with the Abelian field strength pointing in the opposite direction. Such a secondary flux tube is created by wave-like excitations travelling inward from previous locations of the primary peak. In fact, the two-dimensional nature of the bubble-collision problem implied by the $O(1,2)$ symmetry explains why these solutions are similar to waves on a water surface. The trough is less accurately reproduced by the analytical solution as time progresses.

Let us now consider the gauge-invariant Higgs phase $\tilde{\theta} = \int dx^\mu D_\mu \theta$, properly defined in Eq. (23). This phase is equal to the Higgs phase θ_a in the axial gauge. Fig. 6 shows a comparison between the numerical solution for the phase and the analytical solution. As the bubbles collide, the phase in the interior of the bubbles begins to oscillate (to see the location of the bubbles at each time step, refer to Fig. 4a). Note that $\tilde{\theta}$ changes instantly also for large values of $|z|$, which may at first seem unphysical. The phase $\tilde{\theta}$ is, however, a non-local quantity by construction, obtained by integrating the local gauge-invariant phase gradient $D_\mu \theta$. One can check that $D_\mu \theta$ is non-zero only within the causal future of bubble-wall intersections, as should be expected from a physical quantity. Although $\tilde{\theta}$ has no direct physical meaning, it provides a useful, gauge-invariant characterisation of the field configuration, by means of which different solutions can be easily compared. It is also a very sensitive measure, because small deviations in $D_\mu \theta$ accumulate as they are integrated. The agreement between the numerical and analytical solutions in Fig. 6 is nevertheless quite good. Through careful study one finds that the analytical solution is slightly delayed in time after the collision, and also that the amplitude of oscillation is smaller in the analytical solution than in the numerical evolution. We believe that these small deviations are the result of non-linear evolution near the time of collision that our analytical approach is unable to account for.

A particularly interesting quantity is the gauge-invariant phase difference of the two bubbles. For $\tau > t_c$ this is obtained by considering the $z \rightarrow \pm\infty$ limits of Eq. (73), while Eqs. (42), (63) and (49) in the same limits give the result for $\tau < t_c$. With the definition

⁵In fact, the agreement is even better than it appears to be because, in order to produce black-and-white surface graphs such as these, one must use a sparse mesh which cannot always be brought to coincide precisely with peaks and other features.

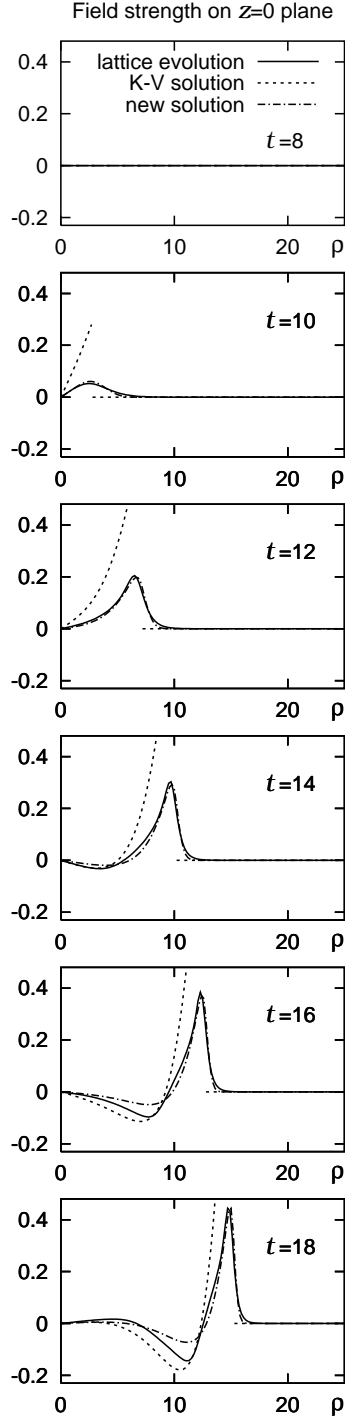


Figure 5: Field strength B^φ (in units of m^2/e) on the plane of symmetry $z = 0$. The numerical solution (solid curve) is compared with the Kibble-Vilenkin approximate solution (dashed) and with our new analytical solution (dot-dashed). For $t \geq 12$, the Kibble-Vilenkin solution extends to higher values of B^φ than what is visible in the graph.

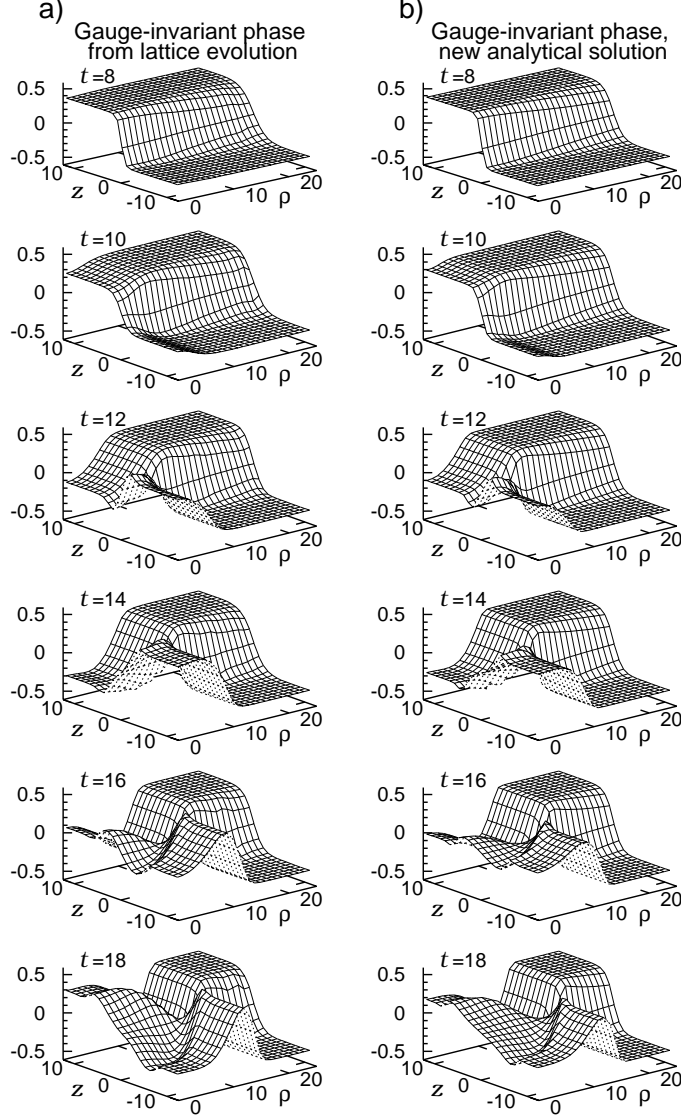


Figure 6: Gauge-invariant phase $\tilde{\theta} = \int dx^\mu D_\mu \theta$ in a bubble collision with initial Higgs-field phase difference $\Delta\theta_0 = 2\theta_0 = \pi/4$: a) Lattice evolution of $\tilde{\theta}$, b) Our new analytical solution for $\tilde{\theta}$. Again, $\rho = (x^2 + y^2)^{1/2}$ is the distance from the symmetry axis of the collision and ρ, z, t are measured in units of $\lambda^{-1/2}\eta^{-1}$. The bubbles first collide at time $t_c = 9.62$, which falls between the first and second frames in each column.

$\Delta\tilde{\theta}(\tau) \equiv \tilde{\theta}(\tau, z \rightarrow +\infty) - \tilde{\theta}(\tau, z \rightarrow -\infty)$ we find

$$\begin{aligned} \Delta\tilde{\theta}(\tau) = \frac{2t_c}{\tau} & \left[\left(\theta_0 - \frac{\sin 2\theta_0}{2} \frac{\beta^2 \pi^2 m^2 t_c^2}{12} \right) \cos m(\tau - t_c) \right. \\ & \left. + \left(\theta_0 - \frac{\sin 2\theta_0}{2} \beta m^2 t_c^2 \right) \frac{\sin m(\tau - t_c)}{mt_c} \right] \quad , \quad \tau > t_c \end{aligned} \quad (76)$$

and

$$\begin{aligned} \Delta\tilde{\theta}(\tau) = 2 & \left[\theta_0 - \frac{\sin 2\theta_0}{2} \beta^2 m^2 t_c^2 \left(\frac{1}{2} \ln(b) \ln \frac{(1-b^2)^2}{b} + \text{Li}_2(b) - \text{Li}_2\left(-\frac{1}{b}\right) - \frac{\pi^2}{6} \right) \right] \\ & , \quad \tau < t_c \end{aligned} \quad (77)$$

where b is defined in Eq. (57). In particular, on the axis through the bubble centres ($\rho = 0$) the phase difference is given by the above expressions with the substitutions $\tau \rightarrow t$ and $b \rightarrow \tilde{b} = \exp[4\mu_c t_c(t - t_c)/R_c]$.

The oscillatory behaviour of the phase difference $\Delta\tilde{\theta}(t)$ after the collision ($t > t_c$) is fully accounted for in Eq. (76). The amplitude of oscillations is proportional to t^{-1} . The phase difference between the interior of the bubbles therefore equilibrates to zero as time progresses. This behaviour was first noted by Kibble and Vilenkin [11]. In fact, in the limit of infinitely thin bubble walls ($\beta \rightarrow 0$), Eq. (76) agrees with Eq. (26), which is their result. On the other hand, the phase difference far from the symmetry axis remains $2\theta_0$. This is evident in Fig. 6a, but also follows analytically from Eq. (77) in the $b \rightarrow 0$ limit, using Eq. (B.4) of Appendix B.

Finally, we shall derive the total flux of the Abelian field strength. This is the flux through a semi-infinite plane based on the z axis, and can be computed in analogy with the discussion leading to Eq. (33) by evaluating the line integral of the vector potential A_μ at a constant time t along the closed path ABDEA indicated in Fig 3a. With finite-thickness bubble walls, however, it is necessary to let the z coordinates of points A and B approach $\pm\infty$, and similarly to take the ρ coordinate of points D and E to infinity. Proceeding as in Ref. [11], we realise that the line integral of eA_μ is equal to the line integral of $D_\mu\theta$, since the line integral of $\partial_\mu\theta$ along a closed path vanishes. Moreover, $D_\alpha\theta$ must vanish on the line segments BD and EA, because they are far removed from the causal future of bubble intersections $I^+(C)_t$. Note, however, that $D_z\theta$ is non-zero on the segment ED. This is because the initial condition establishes a phase difference of $2\theta_0$ between D and E, which contributes to $\partial_z\theta_a$. In the axial gauge $A_z = 0$, and we thus obtain

$$\Phi_B(t) = -\frac{1}{e} \left(\int_{AB} + \int_{DE} \right) dx^\mu \partial_\mu \theta_a = \frac{1}{e} (2\theta_0 - \Delta\tilde{\theta}(t)) \quad , \quad (78)$$

where $\Delta\tilde{\theta}$ is given by Eq. (76) or Eq. (77). As a function of time, the Abelian flux rises from zero and performs damped oscillations about the late-time limit $2\theta_0/e$. This asymptotic value agrees with that found for the Kibble-Vilenkin solution in Sec. 3.1.

7 Conclusions

In this paper, we have attempted to provide the most complete analysis to date of the phase equilibration and field-strength evolution that occur in a U(1) gauge theory when two bubbles of true vacuum collide. Our analysis has been motivated by the work of Kibble and Vilenkin [11], and we have been able to go beyond some of their assumptions concerning the initial configuration of the phase of the scalar field. In particular, we have found that a linear superposition ansatz, coupled with smooth bubble profiles arising from bounce solutions to the Euclidean equations of motion, leads to analytical solutions that are in excellent agreement with the full numerical evolution of the fields, at least for small initial phase difference between the two bubbles.

In Sec. 4, we presented the new, smooth analytical solutions for the Abelian field strength and the gauge-invariant phase. They have a number of advantages over solutions obtained in Ref.[11] using the step-function approximation. For example, from the latter one obtains a peak value of the field strength that differs by a factor of four from the correct value obtained in numerical simulations (a factor of sixteen difference in energy density). Moreover, the solutions (26)–(30) derived from the step-function approximation have discontinuities on the future null surface of bubble intersections and so are unable to account for the behaviour of the fields near that surface. The solutions are only valid over limited ranges of the coordinate $\tau = \sqrt{t^2 - x^2 - y^2}$, which means that they provide no information about the field dynamics shortly before the bubble collisions or, at later times, outside the bubble walls. The smooth ansatz that we adopt, on the other hand, allows us to account for the fact that realistic bubble walls of finite width have exponential tails that begin to overlap long before the instant of collision. The overlapping tails initiate the evolution of the phase of the scalar field and of the vector potential, so that it is already in an advanced stage when the collision reaches full impact. The advantage of the smooth approximation becomes manifest in the comparative plots of Figs. 4–6.

An interesting feature emerges in Fig. 5. There appears to be evidence for the existence of alternating positive peaks and negative troughs in the field strength, corresponding to expanding circular flux-tube loops with alternating direction of the field strength. This raises the possibility that we are seeing here an analogy to the suite of alternating vortices and antivortices found by Digal and Srivastava [29] in the collision region of two colliding bubbles in a global U(1) model. Our peaks are not large enough to form defects, because we have set the initial conditions so that the geodesic rule is obeyed, but it seems that our positive and negative peaks may be an “embryo” for such vortex-antivortex configurations. This is supported by the observation that the modulus of the Higgs field appears to have dips at the locations of the big peak and the trailing

anti-peak. In a hard collision, the field strength would be larger and the Higgs modulus would go down to zero in these two places, corresponding to the formation of topological defects.

We should discuss some of the assumptions we have had to make in this article. We have restricted ourselves to $O(1,2)$ -symmetric solutions, but, as we have argued in Sec. 2.2, this symmetry provides a good description in general for all pairs of nucleated bubbles except possibly in the very first stages of their expansion. Throughout our analysis we have kept the radial component of the complex scalar field fixed in the minimum of the potential within the union of the interior of the two bubbles. The validity of this approximation has been checked against the numerical simulations (see Fig. 4) and has been found satisfactory for the range of initial conditions we have adopted. The constraint placed upon us is that we are not really in a position to discuss the collision process involving large initial phase differences, for that is a situation where we would expect large gradient terms to arise and the scalar field to fluctuate wildly away from the vacuum. At the moment, we do not see any obvious way to approach this problem.

The work we have presented here has a number of natural extensions. For example, one can use our approach to obtain smooth and realistic solutions to effective field equations that incorporate the effects of plasma conductivity, and thereby improve on previous results of this kind obtained with the step-function approximation [14, 17]. Alternatively, or perhaps in addition, one can try to include the effects of frictional damping of the bubble walls [21, 22, 23]. This unfortunately makes the problem non-relativistic and reduces the symmetry from $O(1,2)$ to $O(2)$. Therefore, it is likely that a new type of solution, or even approximation, will be needed.

By going beyond the electroweak Standard Model, we could begin discussing the generation of primordial magnetic fields in a first-order transition. We have good estimates for the magnitude and width of the magnetic fields formed from our smooth ansatz. This could be useful in determining the possible success of generating galactic-strength fields from such seeds in the early Universe.

Acknowledgments

O.T. thanks M.J. Lilley and P.M.S. thanks G. Moore for useful discussions. O.T. is grateful to the Yale Center for Theoretical Physics for kind hospitality. This work was supported by the European Commission's TMR programme under Contract No. ERBFMBI-CT97-2697 and the U.K. EPSRC under Grant GR/K50641. E.J.C and P.M.S. were supported by the U.K. PPARC. Some of this work was performed on Origin 200 machines, supported by Silicon Graphics/Cray Research, HEFCE and PPARC.

Appendix A: Lattice Methods

Here we discuss the method used for the numerical evolution of the equations of motion. The method employs the techniques of lattice gauge theory adapted to a Minkowski metric rather than a Euclidean metric. The formalism has been described by Moore [30] for an SU(2) gauge group and was modified to suit our case of interest, a U(1) gauge theory.

We approximate space-time by a Cartesian grid whose nodes are taken to have spatial separation a . Time is discretised with a fundamental time step ha , $h < 1$. Let us also define l_μ to be the lattice spacing in the μ direction, so that $l_0 = ha$ and $l_i = a$, $i = 1, 2, 3$. The quantity l is not a Lorentz vector, and so raising or lowering of indices is purely notational: $l_\mu \equiv l^\mu$. A vector of length l_μ in the μ direction is denoted by $\hat{\mu}$.

We proceed by introducing a unit-modulus complex vector field $V : (\mu, x) \mapsto \text{U}(1)$ such that $V_\mu(x)$ lives on the link between the neighbouring lattice sites x and $x + \hat{\mu}$. A scalar field $\phi : x \mapsto \mathbf{C}$, with $\phi(x)$ living on the node at x , completes the matter content of the model. The vector field living on the links between the sites alters the way the scalar field is transported around the lattice in much the same way as a connection in general relativity affects the transport of tensor quantities. The lattice covariant derivative of $\phi(x)$, $\tilde{D}_\mu \phi$, is defined by

$$\left(\tilde{D}_\mu \phi\right)(x) = \frac{1}{l_\mu} [V_\mu(x)\phi(x + \hat{\mu}) - \phi(x)] . \quad (\text{A.1})$$

Here there is no summation over repeated indices; in the following any summations shall be made explicit. The covariant derivative (A.1) transforms in the same way as the scalar field under a local U(1) transformation provided that we have

$$\begin{aligned} \phi(x) &\longrightarrow \Omega(x)\phi(x) , & \Omega(x) \in \text{U}(1) ; \\ V_\mu(x) &\longrightarrow \Omega(x)V_\mu(x)\Omega^\dagger(x + \hat{\mu}) . \end{aligned} \quad (\text{A.2})$$

We then have the following candidate for a gauge-invariant kinetic term of the scalar field,

$$\sum_\mu \left(\tilde{D}_\mu \phi\right)^\dagger(x) \left(\tilde{D}^\mu \phi\right)(x) . \quad (\text{A.3})$$

A gauge-invariant kinetic term for the complex vector field $V_\mu(x)$ can be found by realising that the quantity

$$V_{\mu\nu}(x) \equiv V_\nu(x)V_\mu(x + \hat{\nu})V_\nu^\dagger(x + \hat{\mu})V_\mu^\dagger(x) \quad (\text{A.4})$$

is gauge-invariant. The relative normalisation of the scalar and vector kinetic terms is determined from the continuum limit $a \rightarrow 0$ by making the identification $V_\mu(x) \equiv$

$\exp(-il_\mu e A_\mu)$. In the limit of small a one obtains⁶

$$(\tilde{D}_\mu \phi)(x) = \partial_\mu \phi(x) - ie A_\mu(x) \phi(x) + \mathcal{O}(a^2), \quad (\text{A.5})$$

$$\text{Re } V_{\mu\nu}(x) = 1 - \frac{1}{2} l_\mu l_\nu a^2 e^2 F_{\mu\nu} F_{\mu\nu} + \mathcal{O}(a^4), \quad (\text{A.6})$$

$$F_{\mu\nu} = \partial_\mu A_\nu - \partial_\nu A_\mu. \quad (\text{A.7})$$

In terms of these quantities we may then write down a lattice action with a discrete version the gauge symmetry that reduces to the continuum U(1) gauge theory as $a \rightarrow 0$.

$$\begin{aligned} \tilde{S} = & \sum_{\substack{\text{sites} \\ \text{and links}}} ha^4 \left\{ \sum_{\mu} \left[\frac{1}{l_\mu^2} (\phi^\dagger(x + \hat{\mu}) V_\mu^\dagger(x) - \phi^\dagger(x)) (V_\mu(x) \phi(x + \hat{\mu}) - \phi(x)) \right] \right. \\ & \left. + \frac{2}{a^2 e^2} \sum_{\mu, \nu} \frac{1}{l_\mu l_\nu} \text{Re} [V_\nu(x) V_\mu(x + \hat{\nu}) V_\nu^\dagger(x + \hat{\mu}) V_\mu^\dagger(x)] - \mathcal{V}(|\phi(x)|) \right\}. \quad (\text{A.8}) \end{aligned}$$

Here \mathcal{V} is the Higgs potential for the scalar field ϕ . The equations of motion are derived by requiring that the lattice analogue of functional differentiation of \tilde{S} vanish with respect to all the fields. These functional derivatives can be calculated using the relations

$$\frac{\delta \phi(x)}{\delta \phi(y)} = \frac{\delta_{x,y}}{ha^4}, \quad (\text{A.9})$$

$$\frac{\delta V_\mu(x)}{\delta V_\nu(y)} = \delta_\mu^\nu \frac{\delta_{x,y}}{ha^4}, \quad (\text{A.10})$$

$$\frac{\delta V_\mu^\dagger(x)}{\delta V_\nu(y)} = -V_\mu^\dagger(x) V_\nu^\dagger(x) \delta_\mu^\nu \frac{\delta_{x,y}}{ha^4}. \quad (\text{A.11})$$

Upon doing so one discovers that the evolution of $\phi(x)$ is not fully determined. This is a consequence of the gauge-invariance of the system and can be remedied by making a gauge choice analogous to the temporal gauge, $V_0 = 1$. The equations of motion are then found to be

$$\begin{aligned} \pi(\underline{x}, t + \Delta t/2) = & \pi(\underline{x}, t - \Delta t/2) \\ & + ha \left\{ \frac{1}{a^2} \sum_i [V_i(\underline{x}, t) \phi(\underline{x} + \hat{i}, t) - 2\phi(\underline{x}, t) + V_i^\dagger(\underline{x} - \hat{i}, t) \phi(\underline{x} - \hat{i}, t)] - \frac{\partial \mathcal{V}}{\partial \phi^\dagger} \right\}, \quad (\text{A.12}) \end{aligned}$$

⁶In this Appendix we use a sign convention for the covariant derivative which is the opposite from that used in the rest of the paper.

$$\begin{aligned}
\text{Im} [E_k(\underline{x}, t + \Delta t/2)] &= \text{Im} [E_k(\underline{x}, t - \Delta t/2)] \\
&+ ha \left\{ \frac{2e}{a} \text{Im} [\phi^\dagger(\underline{x} + \hat{k}, t) V_k^\dagger(\underline{x}, t) \phi(\underline{x}, t)] \right. \\
&\quad - \frac{1}{ea^3} \sum_i \left(V_k(\underline{x}, t) V_i(\underline{x} + \hat{k}, t) V_k^\dagger(\underline{x} + \hat{i}, t) V_i^\dagger(\underline{x}, t) \right. \\
&\quad \left. \left. + V_i(\underline{x} - \hat{i}, t) V_k(\underline{x}, t) V_i^\dagger(\underline{x} + \hat{k} - \hat{i}, t) V_k^\dagger(\underline{x} - \hat{i}, t) \right) \right\} .
\end{aligned} \tag{A.13}$$

In writing this we have found it convenient to define the quantities $\pi(x)$ and $E_i(x)$ through the relations

$$\phi(\underline{x}, t + \Delta t) = \phi(\underline{x}, t) + ha\pi(\underline{x}, t + \Delta t/2) , \tag{A.14}$$

$$V_i(\underline{x}, t + \Delta t) = ea^2 h E_i(\underline{x}, t + \Delta t/2) V_i(\underline{x}, t) . \tag{A.15}$$

Eqns. (A.12)–(A.15) define a leap-frog algorithm where the canonical momenta, $\pi(x)$ and $E_i(x)$, are defined on time slices half-way between the time slices where the fields live. Note that (A.13) only shows how to evolve the imaginary part of E_i . To get the full evolution we use the fact that V_i has unit modulus; Eq. (A.15) therefore gives $|E_i| = 1/(ea^2 h)$, which fixes the real part of E_i up to a sign. To determine the sign we write $E_k = E_k^{\text{Re}} + iE_k^{\text{Im}}$ and substitute $V_k = \exp(-ieaA_k)$ into (A.15), finding to lowest order in h :

$$\exp(-ieaA_k - iea^2 h \dot{A}_k) \sim ea^2 h (E_k^{\text{Re}} + iE_k^{\text{Im}}) \exp(-ieaA_k) , \tag{A.16}$$

i.e.,

$$1 - iea^2 h \dot{A}_k \sim ea^2 h (E_k^{\text{Re}} + iE_k^{\text{Im}}) . \tag{A.17}$$

We find therefore that in the small- h limit the sensible sign for the real part of eE_k is positive. The sign of the charge e is defined by matching Eq. (A.5) to the usual covariant derivative in the continuum limit. This completes the evolution equations. The equation found by varying the action with respect to V_0 gives the following lattice Gauss constraint,

$$\begin{aligned}
\frac{1}{a} \sum_i \text{Im} [E_i(x, t + \Delta t/2) - E_i(x - \hat{i}, t + \Delta t/2)] &= \\
2e \text{Im} [\pi^\dagger(x, t + \Delta t/2) \phi(x, t)] , &
\end{aligned} \tag{A.18}$$

which is naturally satisfied because the action is invariant under the discrete version of the gauge symmetry, Eq. (A.2).

When working on the lattice one must find appropriate lattice quantities which reduce to the objects under study in the continuum limit. In this work we have been particularly interested in the variation of the phase of the scalar field. The gauge-invariant gradient

of the phase is essentially equal to the Nöther current. This gives us the motivation for defining the lattice covariant derivative of the phase

$$\tilde{D}\theta = \frac{i}{2\phi^\dagger\phi} \left((\tilde{D}\phi)^\dagger\phi - \phi^\dagger\tilde{D}\phi \right) , \quad (\text{A.19})$$

which is clearly gauge-invariant. For the lattice version of the Abelian field strength we use the relation

$$\text{Im } V_{\mu\nu} = el_\mu l_\nu F_{\mu\nu} + \mathcal{O}(a^4), \quad (\text{A.20})$$

which motivates the lattice definition of the field strength as

$$\tilde{B}_i = \frac{1}{2ea^2} \epsilon_{ijk} \text{Im } V_{jk}. \quad (\text{A.21})$$

Appendix B: Polylogarithms

The poly-logarithm function $\text{Li}_n(z)$ is defined by

$$\text{Li}_n(z) = \frac{(-1)^n}{(n-1)!} \int_0^1 dx \frac{\ln^{n-1} x}{x-1/z} = \sum_{k=1}^{\infty} \frac{z^k}{k^n}. \quad (\text{B.1})$$

For real z and integer n the power series is convergent for $-1 \leq z < 1$, $n > 0$ and for $z = 1$, $n > 1$. The functions $\text{Li}_n(z)$ are real-valued for $z \leq 1$. In the case $n = 2$ it is convenient to use the functional relations

$$\text{Li}_2(z) = \begin{cases} -\text{Li}_2(1-z) + \frac{\pi^2}{6} - \ln z \ln(1-z), & \frac{1}{2} < z \leq 1 \\ \text{Li}_2\left(\frac{1}{1-z}\right) - \frac{\pi^2}{6} + \frac{1}{2} \ln^2 \frac{1-z}{|z|} - \frac{1}{2} \ln^2 |z|, & z < -1 \\ -\text{Li}_2\left(\frac{|z|}{1-z}\right) - \frac{1}{2} \ln^2(1-z), & -1 \leq z < 0. \end{cases} \quad (\text{B.2})$$

to express $\text{Li}_2(z)$ in terms of functions $\text{Li}_2(w)$ where $0 \leq w \leq 1/2$. For such w the power series in Eq. (B.1) converges rapidly. For general complex z we also have the following relations:

$$\text{Li}_2(z) + \text{Li}_2(1-z) = \frac{\pi^2}{6} - \ln z \ln(1-z), \quad (\text{B.3})$$

$$\text{Li}_2(z) + \text{Li}_2\left(\frac{1}{z}\right) = -\frac{\pi^2}{6} - \frac{1}{2} \ln^2(-z), \quad (\text{B.4})$$

From Eqs. (B.4) and (B.1) it follows that the dilogarithm function Li_2 has the following asymptotic behaviour:

$$\text{Li}_2(x) \rightarrow -\frac{1}{2} \ln^2(-x) - \frac{\pi^2}{6}, \quad x \rightarrow -\infty. \quad (\text{B.5})$$

More relations between Li_2 functions are given in Ref. [28].

References

- [1] A. Vilenkin and E.P.S. Shellard, *Cosmic Strings and Other Topological Defects* (Cambridge University Press, 1994).
- [2] T. Vachaspati and G. E. Volovik, Int. J. Mod. Phys. B **10**, 471 (1996).
- [3] A. Guth, Phys. Rev. D **23**, 347 (1981).
- [4] Daile La and P. Steinhardt, Phys. Rev. Lett. **62**, 376 (1989); Erratum *ibid.* **62** 1066 (1989).
- [5] D. Lyth and E. Stewart, Phys. Rev. Lett. **75**, 201 (1995).
- [6] Bao-Hua Liu, L. McLerran, and N. Turok, Phys. Rev. D **46**, 2668 (1992).
- [7] M. Laine and K. Rummukainen, Phys. Rev. Lett. **80**, 5259 (1998); J.M. Cline and G.D. Moore, Phys. Rev. Lett. **81**, 3315 (1998).
- [8] S. Hawking, I. Moss, and J. Stewart, Phys. Rev. D **26**, 2681 (1982).
- [9] S. Rudaz and A. Srivastava, Mod. Phys. Lett. A **8**, 1443 (1993).
- [10] M. Hindmarsh, A.-C. Davis, and R. Brandenberger, Phys. Rev. D **49**, 1944 (1994).
- [11] T. Kibble and A. Vilenkin, Phys. Rev. D **52**, 679 (1995).
- [12] E. Copeland and P. Saffin, Phys. Rev. D **54**, 6088 (1996).
- [13] P. Saffin and E. Copeland, Phys. Rev. D **56**, 1215 (1997).
- [14] T. Kibble, J. Phys. A **9**, 1387 (1976).
- [15] I. Chuang, R. Durrer, N. Turok, and B. Yurke, Science **251**, 1336 (1991).
- [16] J. Ye and R. Brandenberger, Mod. Phys. Lett. A **5**, 157 (1990); A. Srivastava, Phys. Rev. D **45**, R3304 (1992); *ibid.* D **46**, 1353 (1992).

- [17] K. J. Ahonen and K. Enqvist, Phys. Rev. D **57**, 664 (1998).
- [18] O. Törnkvist, Phys. Rev. D **58**, 043501 (1998).
- [19] O. Törnkvist, hep-ph/9902432, in *Proceedings of the International Conference on Strong and Electroweak Matter (SEWM-98)*, Copenhagen, Denmark, 2-5 Dec 1998 (World Scientific).
- [20] A.-C. Davis, M. Lilley, and O. Törnkvist, Phys. Rev. D **60**, 021301 (1999), astro-ph/9904022.
- [21] A. Ferrera and A. Melfo, Phys. Rev. D **53**, 6852 (1996).
- [22] M. Joyce, T. Prokopec, and N. Turok, Phys. Rev. D **53**, 2930 (1996).
- [23] A.-C. Davis and M. Lilley, *Damped Bubble Collisions in First-Order Phase Transitions*, Cambridge preprint DAMTP-1999-87.
- [24] S. Coleman, Phys. Rev. D **15**, 2929 (1977); Erratum *ibid.* D **16**, 1248 (1977).
- [25] J. Garriga, Phys. Rev. D **49**, 5497 (1994).
- [26] B. Gidas, W. Ni, and L. Nirenberg, Comm. Math. Phys. **68**, 209 (1979).
- [27] B. de Wit and J. Smith, *Field Theory in Particle Physics*, Vol. 1 (Elsevier, Amsterdam, 1986), Appendix D.
- [28] L. Lewin, *Polylogarithms and Associated functions* (North Holland, 1981).
- [29] S. Digal and A.M. Srivastava, Phys. Rev. Lett. **76**, 583 (1996).
- [30] G. D. Moore, Nucl. Phys. B **480**, 657 (1996); *ibid.* B **480**, 689 (1996).
- [31] H. Kurki-Suonio and M. Laine, Phys. Rev. Lett. **77**, 3951 (1996).